Journal of Sound and Vibration 449 (2019) 274–299

Contents lists available at ScienceDirect

Journal of Sound and Vibration

journal homepage: www.elsevier.com/locate/jsvi

Design and experiment of nonlinear absorber for equal-peak and de-nonlinearity

Xiuting Sun [a], Jian Xu [a, b, *], Feng Wang [a], Li Cheng [c]

[a] School of Aerospace Engineering and Applied Mechanics, Tongji University, Shanghai, PR China
[b] Institute of AI and Robotics, Fudan University, Shanghai, PR China
[c] Department of Mechanical Engineering, The Hong Kong Polytechnic University, Hong Kong, China

ARTICLE INFO

Article history:
Received 15 July 2018
Received in revised form 4 February 2019
Accepted 23 February 2019
Available online 27 February 2019
Handling Editor: I. Lopez Arteaga

Keywords:
Nonlinear tunable vibration absorber
Equal-peak property
De-nonlinearity property
Origami mechanism

ABSTRACT

This paper generalizes and modifies the Equal-peak method for the design of nonlinear vibration absorber for use in the vibration suppression of nonlinear primary vibration system. For a vibration system with nonlinearity, the most relevant bandwidth is the resonance band, in which the undesirable nonlinear vibration phenomenon occurs because of the dramatically amplified of vibration amplitude. To generalize the Equal-peak method for a complex nonlinear primary system under force/base excitations, we utilize the nonlinear perturbation method and bifurcation theory to investigate the vibration performances and critical conditions for dynamical transition. In addition to the Equal-peak property, another novel advantage, called De-nonlinearity (introduced by coupling nonlinearity), is revealed for vibration control in addition to the known effect of nonlinearity on vibration suppression. It is discovered that by applying the nonlinear vibration absorber with appropriate design on the NL primary system, the Equal-peak property can be accurately realized, and unexpected nonlinear vibration performances can be effectively eliminated. A relevant experimental prototype is carried out to illustrate the Equal-peak and De-nonlinearity properties, which is composed of a primary vibration system with complex nonlinearity and a designed tunable nonlinear vibration absorber. The proposed modified design method for Equal-peak and De-nonlinearity properties has huge potential application in the vibration suppression for low-frequency and strong nonlinearity fields such as ships, aircrafts and ocean platform.

1. Introduction

The vibration performances of nonlinear (NL) vibration systems may include some beneficial dynamical phenomenon, such as High-Static-Low-Dynamic and saturation properties, which cannot exist for linear vibration systems [1,2]. Because of the increasing interest in the exploration of novel vibration systems in the fields of aerospace, shipping engineering and ocean platform, nonlinearity is widely utilized in relevant applications [3–6]. However, nonlinearity can introduce undesired complex vibration phenomenon, which usually occurs around the resonance frequency bands because of the large vibration energy induced by resonance. Therefore, vibration absorber (VA) with designed of resonance frequency and nonlinearity is introduced for vibration suppression at the resonance of the nonlinear primary system [7–9].

* Corresponding author. School of Aerospace Engineering and Applied Mechanics, Tongji University, Shanghai, PR China.
E-mail address: xujian@tongji.edu.cn (J. Xu).

https://doi.org/10.1016/j.jsv.2019.02.033
0022-460X/

Nomenclature

NL	Nonlinear
QZS	Quasi-zero-stiffness
x_1	Motion of the primary system
$\hat{x}$	Relative motion between the primary system and the absorber
$u(t)$	Force/base excitation
z_0	Base excitation amplitude
G_1	Restoring force function of the primary system
G_2	Restoring force function of the vibration absorber
k_{1l}	Linear stiffness of the primary system
k_{2l}	Linear stiffness of the vibration absorber
c_1	Linear damping coefficient of the primary system
c_2	Linear damping coefficient of the vibration absorber
k_{1ni}	Nonlinear stiffness coefficient of the primary system
k_{2n}	Nonlinear stiffness coefficient of the vibration absorber
μ	Mass ratio M_2/M_1
Ω_{r1}	The first resonance frequency
Ω_{r2}	The second resonance frequency
Ω_{bi}	The frequency point for jumping on the amplitude-frequency curve
NL-VA	Nonlinear vibration absorber
x_2	Motion of the vibration absorber
f	Force excitation amplitude

The design principle of VA is to induce a channel for vibration energy transformation from the primary system to the absorber. In previous studies, VA with adjustable parameters was considered to be applicable to a wide frequency bandwidth of the primary system. Thus, VA has been mainly designed according to the restoring force of the primary system [7–11]. For an NL primary system, the resonance frequency migrates and is different from the value calculated according to the linear regression part. The nonlinear vibration frequency depends on the vibration response. Therefore, to obtain satisfactory vibration suppression effectiveness for a nonlinear primary system, Nonlinear Vibration Absorbers (NL-VAs) are proposed and designed based on different suppression mechanisms, including autoparametric resonance [12–16] and energy sink [17–19]. To improve the vibration suppression at the resonance band of the primary system, the nonlinearity of NL-VA is designed for the internal resonance. The natural frequency of VA is chosen to be close to the integral multiple of the natural frequency of the primary system, and then an obvious energy sink is induced.

An effective NL-VA is expected not only to realize an anti-resonance effect at the resonance frequency band but also to suppress the vibration amplitude in resonance band for the elimination of the undersigned complex vibration phenomena, including multi-steady state and jumping phenomena induced by large resonance peaks [20]. After the design of the dynamical frequency of NL-VA, the other coefficients of NL-VA are taken into consideration for remarkable vibration suppression on the frequency domain. The Den Hartog's Equal-peak method has been proposed and subsequently widely used for designing the parameters of the Linear Vibration Absorber (L-VA) to realize the H_∞ optimization of the vibration responses on the frequency domain [21,22]. Next, to develop the nonlinear investigation of the suppression and tuning of nonlinear resonance peaks, this Equal-peak method is generalized for the design and optimization of NL-VA for the nonlinear primary system under different amplitudes of the force excitation [23–27]. The generalization of the Equal-peak method on the Duffing primary system is a significant study because it provides the achievement of H_∞ optimization on the frequency domain. In the previous studies of the Equal-peak method, although an appropriately designed NL-VA can make the resonance peaks equal for large range of excitation amplitudes, this existing nonlinear generalization is only feasible for the case that the primary system is a Duffing oscillator and the calculation of the existing tuning method for the Equal-peak property is too large to be generalized further.

In this research, we plan to develop the design method of NL-VA for Equal-peak for the improvement of accuracy and application based on nonlinear perturbation theory and bifurcation theory [28]. The modified design method can be applicable to a NL primary vibration system with multiple terms of nonlinearity for force/base excitations. The designed NL-VA can accurately realize the Equal-peak property for as large as possible ranges of the structural and excitation parameters. For example, for the so-called Quasi-Zero-Stiffness (QZS) vibration systems [20,29–34], which is required to have high-static-low-frequency (HSLF) property, a large resonance peak exists at this low frequency band and its restoring force is a complex nonlinear function of the motion. Thus, the designed VA can be applied on these primary systems to suppress the vibration, especially on the resonance frequency band. On the other hand, for a modelled nonlinear vibration system in engineering practices, such as architectural structures, ship structures and aircraft truss structures, the configurations and

elastic components cannot be changed easily to eliminate the undesired nonlinear phenomenon. This study on avoiding nonlinear vibration performances is inspired by the previous studies on the concept of de-nonlinearity [9,21]. In Ref. [9], nonlinearity induced by magnetic interaction is added on a nonlinear continuous structure. It proposes the concept that the introduction and design of nonlinearity can avoid the nonlinear vibration performances of the primary system. In Ref. [22], it discovers that the amplitude-frequency curve of a nonlinear primary system is similar as a linear system by introducing appropriate nonlinear and damping coefficients of VA. In this paper, the studies on the transition of dynamical performances such as multi-steady states regions show the mechanism of De-nonlinearity property due to the nonlinearity of the absorber. Adding NL-VA with the simple Duffing nonlinearity can effectively allow the nonlinear primary system to perform as a linear one by cutting the curves of resonance peak for multi-terms nonlinearity. The experimental prototype of the NL-VA, which is assembled and realized by utilizing the Origami mechanism, also demonstrates the novelty of this research [35,36]. For the Origami structure, the nonlinearity can be adjusted according to the designed parameters obtained by the proposed modified method.

The paper is organized as follows. First, the principle and existing inadequacy of the Equal-peak method for NL-VA are introduced in Section 2. Next, a modified tuning method with a derivation process is proposed based on HBM and bifurcation analysis. With the comparison of results obtained by the modified method and the previous method, the parametrical design of NL-VA by the modified method is found to be more effective and accurate in Section 3. In addition, it is verified that the modified method is applicable for NL primary system under force/base excitations by the cases for the seventh-order nonlinear vibration oscillator and the one with multiple nonlinear terms. Last, the experimental prototype of the NL-VA applied on primary system with QZS property is realized by the Origami structure in Section 4 for the effect verification of the Equal-peak and De-nonlinearity properties. The conclusion is given in the final Section.

2. The design principle of the nonlinear vibration absorber (NL-VA)

From the results obtained by the previous studies [7–9,23–26], a tunable VA with adjustable stiffness and damping is proposed to suppress the vibration over a wide frequency band for a linear primary vibration system. To mitigate the nonlinear resonance for as large as possible a range of forcing amplitudes, the full exploitation of the NL-VA is investigated when the primary system is a nonlinear oscillator. The mechanical diagram is shown in Fig. 1.

As shown in Fig. 1, NL-VA is assembled on a NL primary system, which is composed of a two-degree-of-freedom (2-DOF) vibration system. According to the mechanical model shown in Fig. 1, the dynamical equation of the 2-DOF system is

$$\begin{aligned} &M_1\ddot{x}_1 + G_1(x_1) + c_1\dot{x}_1 + G_2(x_1 - x_2) + c_2(\dot{x}_1 - \dot{x}_2) = u(t), \\ &M_2\ddot{x}_2 - G_2(x_1 - x_2) + c_2(\dot{x}_2 - \dot{x}_1) = 0. \end{aligned} \tag{1}$$

where G_1 and G_2 are the nonlinear restoring forces for the primary system and the VA, respectively. The previous studies [8,9,24] considered that the third-order Taylor series can describe the nonlinearity. Thus, the dynamical equation is simplified for a coupled system with Duffing nonlinearity. Substituting $\hat{x} = x_1 - x_2$ into Eq. (1), the dynamical equation is written as

$$\begin{aligned} &M_1\ddot{x}_1 + k_{1l}x_1 + k_{1n}x_1^3 + c_1\dot{x}_1 + k_{2l}\hat{x} + k_{2n}\hat{x}^3 + c_2\dot{\hat{x}} = u(t), \\ &M_2\ddot{\hat{x}} + \mu k_{1l}x_1 + \mu c_1\dot{x}_1 + \mu k_{1n}x_1^3 \\ &\quad + (\mu+1)k_{2l}\hat{x} + (\mu+1)k_{2n}\hat{x}^3 + (\mu+1)c_2\dot{\hat{x}} = \mu u(t), \end{aligned} \tag{2}$$

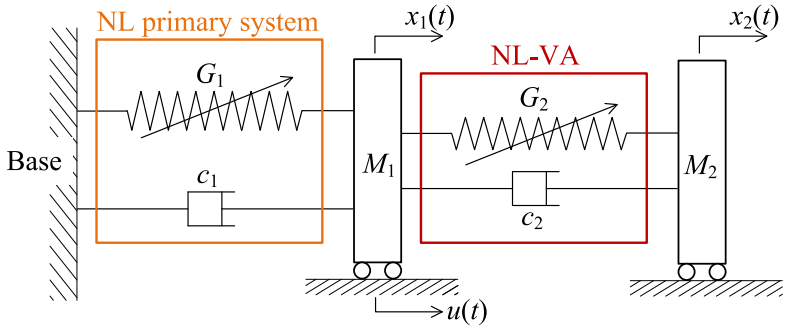

Fig. 1. Mechanical diagram of the vibration system consisting of the NL primary oscillator and the NL-VA.

where $\mu = \frac{M_2}{M_1}$, $k_{1n} = \left.\frac{d^3G_1}{dx_1^3}\right|_{x_1=0}$, $k_{2n} = \left.\frac{d^3G_2}{d\hat{x}^3}\right|_{\hat{x}=0}$ and $u(t)$ is excitation as $u(t) = f\cos\omega t + \phi_1$. The derivation from Eq. (1) to Eq. (2) is shown in Appendix A.

Introducing the dimensionless parametrical transformation as

$$\begin{aligned} &\tilde{t} = \omega_1 t, \omega_1 = \sqrt{\frac{k_{1l}}{M_1}}, \omega_2 = \sqrt{\frac{k_{2l}}{M_2}}, \gamma = \frac{\omega_2}{\omega_1}, 2\xi_1 = \frac{c_1}{M_1\omega_1}, 2\xi_2 = \frac{c_2}{M_2\omega_2}, \\ &f = \frac{F}{k_{1l}}, \alpha = \frac{k_{1n}}{k_{1l}}f^2, \beta = \frac{k_{2n}}{M_2\omega_1^2}f^2, \Omega = \frac{\omega}{\omega_1}, \mu = \frac{M_2}{M_1}, \end{aligned} \tag{3}$$

the dimensionless dynamical equation is

$$\begin{aligned} &x_1'' + x_1 + \alpha x_1^3 + 2\xi_1 x_1' + \mu\gamma^2(\hat{x} - x_1) + \mu\beta(\hat{x} - x_1)^3 + 2\xi_2\mu\gamma(\hat{x}' - x_1') = \cos(\Omega\tilde{t} + \phi_1), \\ &\hat{x}'' + x_1 + \alpha x_1^3 + 2\xi_1 x_1' + (\mu+1)\gamma^2(\hat{x} - x_1) + (\mu+1)\beta(\hat{x} - x_1)^3 + 2(\mu+1)\xi_2\gamma(\hat{x}' - x_1') = \cos(\Omega\tilde{t} + \phi_1). \end{aligned} \tag{4}$$

The detailed derivation of Eq. (4) under dimensionless parameters is also shown in Appendix A. According to the previous studies of the Equal-peak method [23,24], for the Duffing primary system with fixed M_1, k_{1l}, c_1 and k_{1n}, to realize the Equal-peak property, the structural parameters M_2, k_{2l}, c_2 and k_{2n} of the NL-VA should be designed as

$$\begin{aligned} &M_2 = \mu M_1, \\ &k_{2l} = \frac{8\mu k_{1l}\left[16 + 32\mu + 9\mu^2 + 2(2+\mu)\sqrt{4+3\mu}\right]}{3(1+\mu)^2\left(64 + 80\mu + 27\mu^2\right)}, \\ &c_2 = \sqrt{\frac{k_{2l}M_2\left(8 + 9\mu - 4\sqrt{4+3\mu}\right)}{4(1+\mu)}}, \\ &k_{2n} = \frac{2\mu^2 k_{1n}}{1+4\mu}. \end{aligned} \tag{5}$$

Eq. (5) reveals that the values of k_{1n} and k_{2n} are approximately in a linear relationship for the Equal-peak property. Thus, according to the previous studies [23,24], regardless of the excitation amplitude of f, the nonlinear coefficient k_{2n} of NL-VA is considered proportional to the nonlinear coefficient k_{1n} of the primary system. We increase the excitation amplitude f and nonlinear coefficient k_{1n} to examine the accuracy of the existing approach. To increase f and k_{1n} over wide ranges while fixing parameters according to Eq. (5), the amplitude responses of the primary system on the frequency band are shown in Fig. 2.

From Fig. 2, it can be seen that the amplitudes of the primary system in the frequency domain can be controlled to a low range by applying the NL-VA. The resonance peaks can be effectively reduced by increasing the nonlinear coefficient k_{2n} proportionally to k_{1n} for a larger f. However, as shown in Fig. 2, we can also see that when the values of f and k_{1n} are increased further, the values of the two resonance peaks are unequal and the phenomenon of multi-steady states occurs.

The tuning method for the Equal-peak condition is significant for vibration suppression. However, there are three main deficiencies for the existing approach to determine the optimum nonlinear coefficient of NL-VA. First, the previous method requires a massive amount of calculation because we must obtain all the amplitudes around the resonance frequencies for different values of the other parameters. Second, the optimum nonlinear coefficient of NL-VA is obtained with the other parameters changing in specific ranges rather than over very wide ranges. Third, the existing conclusion in Refs. [23,24] for the designed NL-VA shows that the Equal peak property can be realized for a nonlinear primary system. Based on the previous studies [8,9,23–26], we explore a modified tuning method for nonlinear generalization to determine the optimum nonlinear coefficient of NL-VA for the primary system with multiple nonlinear terms for force/base excitations. The proposed method also should be applicable for other parameters changing over wider ranges compared to those in the previous studies [8,9,23,24].

3. Design of the NL-VA for equal-peak and de-nonlinearity properties

3.1. Method for the design of the NL-VA

In this section, we explore the Equal-peak method of NL-VA for the primary system with nonlinearity under both base and force excitations with as large as possible values for the ranges of excitation amplitude and nonlinear strength. The process for determining the optimum nonlinear coefficients of the NL-VA is based on the nonlinear analysis of the vibration properties.

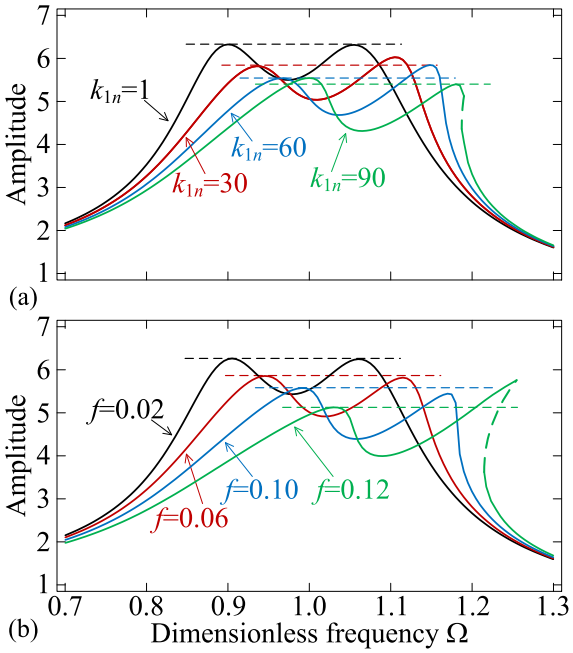

Fig. 2. The amplitude responses of the primary system for (a) increasing k_{1n} by fixing $f=0.005$ and (b) increasing f by fixing $k_{1n}=1$.

3.1.1. Nonlinear resonance frequencies

Considering the nonlinearities of the NL primary system and the NL-VA, the dynamical equation is written as

$$\begin{aligned} &M_1\ddot{x}_1 + k_{1l}x_1 + g_{n1}(x_1) + c_1\dot{x}_1 + k_{2l}\hat{x} + g_{n2}(\hat{x}) + c_2\dot{\hat{x}} = u(t),\\ &M_2\ddot{\hat{x}} + \mu k_{1l}x_1 + \mu c_1\dot{x}_1 + \mu g_{n1}(x_1)\\ &\quad + (\mu+1)k_{2l}\hat{x} + (\mu+1)g_{n2}(\hat{x}) + (\mu+1)c_2\dot{\hat{x}} = u(t), \end{aligned} \tag{6}$$

where g_{n1}, and g_{n2} are the nonlinear restoring forces for the NL primary system and the NL-VA. Without losing the generalization, we write the NL restoring force function as the following polynomial.

$$\begin{cases} g_{n1}(x_1) = \sum_{i=2}^{\infty} k_{1ni}x_1^i,\\ g_{n2}(\hat{x}) = \sum_{i=2}^{\infty} k_{2ni}\hat{x}^i. \end{cases} \tag{7}$$

The excitation $u(t)$ in dynamical Eq. (6) is assumed to be a harmonic signal. For force excitation, $u(t)$ is written as $u(t)=f\cos(\omega t+\phi_1)$, and for base excitation, $u(t)$ is the acceleration applied on M_1 as $u(t)=z_e\omega^2\cos(\omega t+\phi_1)$. For force and base excitations, the theoretical method for the nonlinearity generalization of the Equal-peak property is similar. In this section, to illustrate the modified method for the optimum design of the nonlinearity of the NL-VA, the force excitation $u(t)=f\cos(\omega t+\phi_1)$ is applied as an example.

Introducing the parametrical dimensionless transformation similar to Eq. (3), the dimensionless dynamical equation is written as

$$\begin{aligned} &x_1'' + x_1 + 2\xi_1 x_1' + \sum_{i=2}^{\infty}\alpha_i x_1^i + \mu\gamma^2\hat{x} + \mu\sum_{i=2}^{\infty}\beta_i\hat{x}^i + 2\xi_2\mu\gamma\hat{x}' = \cos(\Omega\tilde{t}+\phi_1),\\ &\hat{x}'' + x_1 + 2\xi_1 x_1' + \sum_{i=2}^{\infty}\alpha_i x_1^i\\ &\quad + (\mu+1)\gamma^2\hat{x} + (\mu+1)\sum_{i=2}^{\infty}\beta_i\hat{x}^i + 2(\mu+1)\xi_2\gamma\hat{x}' = \cos(\Omega\tilde{t}+\phi_1). \end{aligned} \tag{8}$$

The coefficients in the polynomial expressions (8) are $\alpha_i = \frac{k_{1ni}}{k_{1l}} f^{i-1}$ and $\beta_i = \frac{k_{2ni}}{M_2 \omega_1^2} f^{i-1}$ ($i = 2,3, \ldots$). Utilizing HBM with high-order harmonics, the solutions of the primary system and NL-VA are written as

$$\begin{cases} x_1 = a_0 + a_1 \cos(\Omega\tilde{t}) + \sum_{k=2} [a_{k1} \cos(k\Omega\tilde{t}) + a_{k2} \sin(k\Omega\tilde{t})], \\ \hat{x} = b_0 + \sum_{k=1} [b_{k1} \cos(k\Omega\tilde{t}) + b_{k2} \sin(k\Omega\tilde{t})]. \end{cases} \tag{9}$$

Because we consider multiple nonlinear terms in the study, the expression of the solution contains high-order harmonics for convergence and accuracy. The high-order harmonic terms correct the accuracy of the amplitude at the fundamental frequency. The amplitude of the primary system at the fundamental frequency a_1 is the design criterion for the NL-VA. The relationship between the fundamental frequency amplitudes and the frequency should be obtained not only for the solution but also for stability analysis. Therefore, in Eq. (9), we set the amplitudes a_1 and b_1 in polar form and the high-order harmonic in rectangular form. In all, there are $2(K-2)+2$ unknown amplitude coefficients a_0, a_1, a_{k1} and a_{k2} ($k = 2,3, \ldots,K$) in x_1 and $2(K-1)+1$ unknown amplitude coefficients b_0, b_{k1} and b_{k2} ($k = 1,2, \ldots,K$) in x_2.

Substituting the HBM solution (9) into dynamical Eq. (8), we obtain the conditions that the constant terms and the coefficient functions for each-order harmonic should equal to zero. From the first equation of Eq. (8), the constant terms obtained are expressed by the function H_{10}; the expressions of $\cos\phi_1$ and $\sin\phi_1$ are solved by the coefficient functions for $\cos \Omega\tilde{t}$ and $\sin \Omega\tilde{t}$, respectively, and then, the function obtained by the condition of trigonometric function as $\cos^2\phi_1 + \sin^2\phi_1 = 1$ is H_1; according to the condition that the coefficient for each-harmonic term should be zero, we can obtain the functions H_{ak1}, H_{ak2} ($k = 2,3, \ldots,K$). Thus, there can obtain $2(K-2)+2$ equations from the first equation of Eq. (8). Similarly, from the second equation of Eq. (8), the constant terms obtained are expressed by the function H_{20}; the functions H_{bk1}, H_{bk2} ($k = 1,2, \ldots,K$) express the coefficient for each harmonic. In all, there can obtain $2(K-1)+1$ from the second equation of Eq. (8).

Therefore, in total, for K order harmonics, we have $4K + 1$ unknown amplitude coefficients and $4K + 1$ nonlinear algebraic equations from Eq. (8). Thus, all the amplitudes can be calculated. The nonlinear algebraic equations are H_{10}, H_1, H_{ak1}, H_{ak2} ($k = 2,3, \ldots,K$) from the first equation of Eq. (8) and H_{20}, H_{bk1}, H_{bk2} ($k = 1,2, \ldots,K$), written as

$$\begin{cases} H_{10}(a_0, b_0, a_1, \mathbf{a}, \mathbf{b}, \Omega, \boldsymbol{\kappa}) = 0, \\ H_{20}(a_0, b_0, a_1, \mathbf{a}, \mathbf{b}, \Omega, \boldsymbol{\kappa}) = 0, \\ H_1(a_0, b_0, a_1, \mathbf{a}, \mathbf{b}, \Omega, \boldsymbol{\kappa}) = 1, \\ H_{ak1}(a_0, b_0, a_1, \mathbf{a}, \mathbf{b}, \Omega, \boldsymbol{\kappa}) = 0 \quad 2 \le k \le K, \\ H_{ak2}(a_0, b_0, a_1, \mathbf{a}, \mathbf{b}, \Omega, \boldsymbol{\kappa}) = 0 \quad 2 \le k \le K, \\ H_{bk1}(a_0, b_0, a_1, \mathbf{a}, \mathbf{b}, \Omega, \boldsymbol{\kappa}) = 0 \quad 1 \le k \le K, \\ H_{bk2}(a_0, b_0, a_1, \mathbf{a}, \mathbf{b}, \Omega, \boldsymbol{\kappa}) = 0 \quad 1 \le k \le K, \end{cases} \tag{10}$$

where $\boldsymbol{a}$ and $\boldsymbol{b}$ reflect the amplitude of high-order harmonic as $\boldsymbol{a} = \{a_{21}, a_{22}, \ldots, a_{K1}, a_{K2}\}$, $\boldsymbol{b} = \{b_{11}, b_{12}, b_{21}, b_{22}, \ldots, b_{K1}, b_{K2}\}$, and $\boldsymbol{\kappa}$ represents the nonlinear coefficient of NL-VA to be designed.

The optimum nonlinear coefficient of NL-VA should render the values of two resonance peaks low and equal. The resonance frequencies at the original fundamental frequency band of the primary system are defined as Ω_{r1} and Ω_{r2}, whose values depend on the amplitude of the steady state a_1. Because the primary system and VA are both nonlinear oscillators, with coupling in both linear and nonlinear parts, the accurate values of Ω_{r1} and Ω_{r2} cannot be theoretically expressed by linear eigenvalue analysis. Although Ω_{r1} and Ω_{r2} cannot be expressed explicitly, they always correspond to the extremes on the amplitude-frequency curves expressed by H_1. Therefore, the resonance frequencies Ω_{r1} and Ω_{r2} for the two resonance peaks are defined by the conditions for extremes on the amplitude-frequency curve as

$$\{\Omega_{r1}, \Omega_{r2}\} = \left\{ \Omega_r | \frac{\mathrm{d}H_1(\Omega)}{\mathrm{d}\Omega} = 0 \ \& \frac{\mathrm{d}^2 H_1(\Omega)}{\mathrm{d}\Omega^2} < 0 \right\}. \tag{11}$$

3.1.2. Multi-steady states frequency bandwidths

Alternatively, as shown in Fig. 2 (b), when the excitation amplitude and nonlinearity strength are increased, the phenomenon of multi-steady states occurs. As shown in the previous studies about nonlinear vibration systems, on the frequency band, at critical frequencies for multi-steady states, one solution may bifurcate to three solutions [2–4,8,9,17–30]. The critical frequencies, defined as Ω_{bi} ($i = 1,2, \ldots$), correspond to the local saddle-node bifurcation of the solution. According to the bifurcation theory for determining the saddle-node point of the steady states, the values of the critical frequency Ω_{bi} satisfy the following condition

$$\{\Omega_{bi}\} = \left\{ \Omega_{bi} | \frac{\mathrm{d}H_1(a_1, \Omega)}{\mathrm{d}a_1} = 0 \right\}. \tag{12}$$

The number of Ω_b depends on the parameters of the system. For small f and k_{1ni}, there is no multi-steady state band; for increasing f and $k_{1ni,}$ the multi-steady states may occur. When the NL-VA is applied in the primary system, the bandwidth of multi-steady states is reduced for increasing the nonlinear coefficient k_{2n}. However, for further increasing the k_{2n}, the other resonance peak is raised, and thus, the multi-steady states may occur again. Therefore, by considering the values and occurrence of Ω_{r1}, Ω_{r2} and Ω_{bi}, the optimum design of nonlinearity of NL-VA can be obtained theoretically, thereby mitigating the vibration responses in the resonance band as well as eliminating the multi-steady states.

3.2. Derivation process of the modified method on the design of NL-VA

From the analysis in the above section, the amplitude-frequency curve at the fundamental frequency band is determined by all the equations in Eq. (10); the nonlinear resonance frequencies satisfy Eq. (11); and the frequency bandwidth for multi-steady states satisfies Eq. (12). We show these critical points and curves in Fig. 3 to illustrate the principle of the method.

Fig. 3 illustrates the principle of the curves Ω_{r1} and Ω_{r2} and the points Ω_{bi}. The proposed method for the nonlinear generalization and optimization design of NL-VA is based on the curves and points shown in Fig. 3. Although the expressions of Eq. (10), Ω_{r1}, Ω_{r2} and Ω_{bi} are complex, all the formulas are implicit algebraic polynomial equations, which have indicated roots. Thus, for complex nonlinearity or large excitation amplitudes, the accurate optimal nonlinear coefficients of NL-VA that achieve the requirements of suppression effectiveness can be obtained.

As illustrated in Fig. 3, the critical condition for the Equal-peak property is that the amplitude of the primary system at the first resonance point is equal to the value at the second one. However, the amplitude of VA is different at the two resonance peaks. To realize the Equal-peak property, at the first and second new resonance peaks Ω_{r1} and Ω_{r2} around the original fundamental resonance frequency band, the amplitudes of the primary system are both A_1, and the amplitudes for the high-order harmonics of the primary system and NL-VA are different. The conditions for the Equal-peak property are written as

$$\begin{cases} H_{10}(A_1,\mathbf{a}_1,\mathbf{b}_1,\Omega_{r1},\boldsymbol{\kappa}_c)=0, \\ H_{20}(A_1,\mathbf{a}_1,\mathbf{b}_1,\Omega_{r1},\boldsymbol{\kappa}_c)=0, \\ H_{1}(A_1,\mathbf{a}_1,\mathbf{b}_1,\Omega_{r1},\boldsymbol{\kappa}_c)=1, \\ H_{ak1}(A_1,\mathbf{a}_1,\mathbf{b}_1,\Omega_{r1},\boldsymbol{\kappa}_c)=0 \quad 2\le k\le K, \\ H_{ak2}(A_1,\mathbf{a}_1,\mathbf{b}_1,\Omega_{r1},\boldsymbol{\kappa}_c)=0 \quad 2\le k\le K, \\ H_{bk1}(A_1,\mathbf{a}_1,\mathbf{b}_1,\Omega_{r1},\boldsymbol{\kappa}_c)=0 \quad 1\le k\le K, \\ H_{bk2}(A_1,\mathbf{a}_1,\mathbf{b}_1,\Omega_{r1},\boldsymbol{\kappa}_c)=0 \quad 1\le k\le K, \end{cases} \tag{13a}$$

and

$$\begin{cases} H_{10}(A_1,\mathbf{a}_2,\mathbf{b}_2,\Omega_{r2},\boldsymbol{\kappa}_c)=0, \\ H_{20}(A_1,\mathbf{a}_2,\mathbf{b}_2,\Omega_{r2},\boldsymbol{\kappa}_c)=0, \\ H_{1}(A_1,\mathbf{a}_2,\mathbf{b}_2,\Omega_{r2},\boldsymbol{\kappa}_c)=1, \\ H_{ak1}(A_1,\mathbf{a}_2,\mathbf{b}_2,\Omega_{r2},\boldsymbol{\kappa}_c)=0 \quad 2\le k\le K, \\ H_{ak2}(A_1,\mathbf{a}_2,\mathbf{b}_2,\Omega_{r2},\boldsymbol{\kappa}_c)=0 \quad 2\le k\le K, \\ H_{bk1}(A_1,\mathbf{a}_2,\mathbf{b}_2,\Omega_{r2},\boldsymbol{\kappa}_c)=0 \quad 1\le k\le K, \\ H_{bk2}(A_1,\mathbf{a}_2,\mathbf{b}_2,\Omega_{r2},\boldsymbol{\kappa}_c)=0 \quad 1\le k\le K, \end{cases} \tag{13b}$$

where A_1 is the equal amplitudes of the primary system on Ω_{r1} and Ω_{r2}, $\mathbf{a}_1=\{a_{0\_1},a_{21\_1},a_{22\_1},\ldots,a_{K1\_1},a_{K2\_1}\}$, $\mathbf{a}_2=\{a_{0\_2},a_{21\_2},a_{22\_2},\ldots,a_{K1\_2},a_{K2\_2}\}$, $\mathbf{b}_1=\{b_{0\_1},b_{11\_1},b_{12\_1},\ldots,b_{K1\_1},b_{K2\_1}\}$, $\mathbf{b}_2=\{b_{0\_2},b_{11\_2},b_{12\_2},\ldots,b_{K1\_2},b_{K2\_2}\}$ and $\boldsymbol{\kappa}_c$ reflects the optimal parameters of NL-VA for the Equal-peak property.

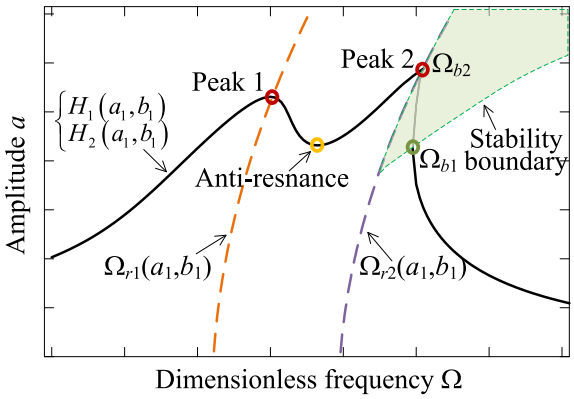

Fig. 3. The amplitude-frequency curve, the nonlinear resonance frequencies, the multi-steady states band and the critical frequency points.

The factor that determines whether the multi-steady states phenomenon occurs is determined by bifurcation theory. When the designed NL-VA can eliminate the frequency bandwidth of multi-steady states, the nonlinearity of NL-VA plays a significant role in erasing the nonlinear performances for the primary system. Here, we define a new concept of De-nonlinearity, i.e., the vibration of a nonlinear oscillator performs similar to a linear oscillator induced by an introduced nonlinearity. Because of the De-nonlinearity property, the NL-VA reduces undesirable nonlinear vibration performances. The critical frequencies Ω_{bi} for multi-steady states and the corresponding amplitude can be solved by the following equations:

$$\begin{cases} H_{10}(a_0, b_0, a_1, \mathbf{a}, \mathbf{b}, \Omega_{bi}, \kappa_c) = 0, \\ H_{20}(a_0, b_0, a_1, \mathbf{a}, \mathbf{b}, \Omega_{bi}, \kappa_c) = 0, \\ H_1(a_0, b_0, a_1, \mathbf{a}, \mathbf{b}, \Omega_{bi}, \kappa_c) = 1, \\ \partial H_1/\partial a_1 = 0, \\ H_{ak1}(a_0, b_0, a_1, \mathbf{a}, \mathbf{b}, \Omega_{bi}, \kappa_c) = 0 \quad 2 \le k \le K, \\ H_{ak2}(a_0, b_0, a_1, \mathbf{a}, \mathbf{b}, \Omega_{bi}, \kappa_c) = 0 \quad 2 \le k \le K, \\ H_{bk1}(a_0, b_0, a_1, \mathbf{a}, \mathbf{b}, \Omega_{bi}, \kappa_c) = 0 \quad 1 \le k \le K, \\ H_{bk2}(a_0, b_0, a_1, \mathbf{a}, \mathbf{b}, \Omega_{bi}, \kappa_c) = 0 \quad 1 \le k \le K, . \end{cases} \tag{14}$$

Eq. (14) determines the boundary for the nonlinear coefficients of NL-VA for multi-/single-steady states and the bandwidth of the multi-steady states.

In summary, when the parameters of primary system are given as M_1, k_{1l}, and c_1 and the nonlinearity g_{n1} is fixed, the parameters in linear terms of the proposed NL-VA are designed as in Refs. [23,24], while the nonlinear coefficients are determined by the proposed method of Eq. (13). In addition, Eq. (14) is utilized to assess the occurrence of the multi-steady states band. The principles and formulas of the proposed method are reorganized as the derivation process shown in Fig. 4.

From Fig. 4, the optimal nonlinear coefficients of NL-VA can be determined to realize the low vibration amplitudes at the resonance frequencies and avoid the unexpected nonlinear vibration phenomenon. According to the process shown in Fig. 4, the NL-VA is applicable for the primary system with multiple nonlinear terms under force/base excitations.

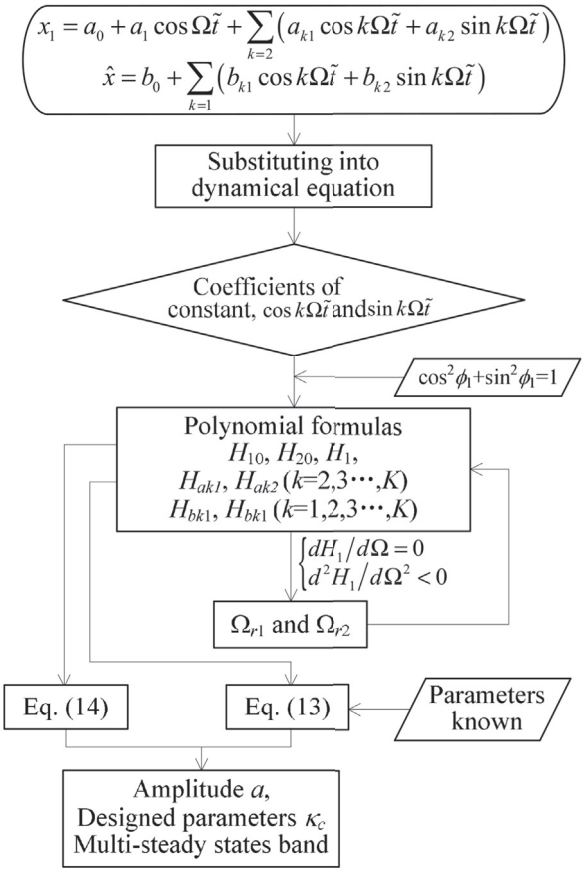

Fig. 4. The derivation process of the proposed method for designing the NL-VA.

3.3. Case studies and comparisons

For a primary system with multiple nonlinear terms, the nonlinearity of NL-VA should be simple but efficient. Thus, the NL-VA is always assumed as a Duffing nonlinear oscillator, and the nonlinear function g_{n2} in the dynamical equation is $g_{n2}(\widehat{x}) = k_{2n}\widehat{x}^3$. The nonlinear coefficient to be designed is only k_{2n}, which can clearly illustrate the accuracy and mechanism of vibration suppression by the NL-VA. The following two case studies show the mechanism and efficiency of a VA with simple nonlinearity on vibration suppression at the fundamental frequency of a primary system with Duffing/multi-terms nonlinearities.

3.3.1. NL-VA on a system with Duffing nonlinearity

To verify the modified tuning method and show its improvement to determine a more accurate design of nonlinear coefficient of NL-VA for the Equal-peak property, in the first case study, we consider the primary system to be a weak nonlinear oscillator. The mechanical model is similar to that shown in Fig. 1, and the dimensionless dynamical equation is expressed in the same manner as Eq. (3). Because of weak nonlinearity, the restoring force is expanded by Taylor series as $g_{n1}(x_1) = \left(\frac{\mathrm{d}^3 G_1}{\mathrm{d}x_1^3}\Big|_{x_1=0}\right)x_1^3 = k_{1n3}x_1^3$. The dimensionless dynamical equation is written as

$$\begin{aligned} &x_1'' + x_1 + 2\xi_1 x_1' + \alpha_3 x_1^3 + \mu\gamma^2\widehat{x} + \mu\beta\widehat{x}_1^3 + 2\xi_2\mu\gamma\widehat{x}' = \cos(\Omega\tilde{t} + \phi_1),\\ &\widehat{x}'' + x_1 + 2\xi_1 x_1' + \alpha_3 x_1^3\\ &\quad +(\mu+1)\gamma^2\widehat{x} + (\mu+1)\beta\widehat{x}_1^3 + 2(\mu+1)\xi_2\gamma\widehat{x}' = \cos(\Omega\tilde{t} + \phi_1), \end{aligned} \tag{15}$$

where $\alpha_3 = \frac{k_{1n3}}{k_{1l}} f^2$, and $\beta = \frac{k_{2n}}{M_2\omega_1^2} f^2$. As a simple case study for the verification of the proposed method, the actual expressions of Eq. (14) for different-order harmonics are listed in Appendix B as Eqs. (B.2)-(B.11).

Assuming that the structural parameters M_1, k_{1l}, k_{1n3}, and c_1 of the primary system are fixed and known, the nonlinear coefficient k_{2n} of the absorber is designed according to the proposed method. When the parameter values of the linear part of the primary system are fixed as $M_1 = 1$, $k_{1l} = 1$, and $c_1 = 0.002$, the values of M_2, k_{2l}, and c_2 of the linear part in the NL-VA are selected according to the conclusions in Ref. [24] (the expressions are shown in Eq. (5)) as $M_2 = \mu M_1 = 0.05$, $k_{2l} = 0.04513$, and $c_2 = 0.0128$. According to the derivation process in Fig. 4, the values of k_{2n} are obtained, as shown in Fig. 5 for different mass ratios μ, nonlinear coefficients k_{1n3} and excitation amplitudes f. In Ref. [24], the ratio between k_{2n} and k_{1n3} is found to be independent of the value of the excitation amplitude f.

The results obtained by the proposed method in Fig. 5 reveal that the ratio between k_{2n} and k_{1n3} is approximately equal to a constant for small f, whereas the ratio deviates from that relationship for large f. Since the nonlinearity of the primary system only contains the cubic term in this case, we refer to Ref. [24] to propose a fitting factor between k_{2n} and k_{1n3} for quickly finding the optimum value k_{2n} for Duffing primary system. Referring the previous study [24] and based on the variations of k_{2n} for the Equal-peak property under different values of f in Fig. 5 (a), a correction factor is introduced to time the factor $2\mu^2/(1+4\mu)$ in Ref. [24], and then, the regression of k_{2n} is given by

$$k_{2n} \approx (1.15 - 4.3f)\frac{2\mu^2}{1+4\mu}k_{1n3}. \tag{16}$$

The optimum values obtained by the regression expressed as Eq. (16) is also shown in Fig. 5.

Fig. 5 shows that the proposed modified method can obtain the accurate nonlinear coefficient of NL-VA for the Equal-peak property. The accurate optimal value of k_{2n} is determined by solving the functions in Eq. (11) according to the expressions of H_1 and H_2, which are given in Appendix B. Thus, the calculation is much smaller than the previous process. For small k_{1n3}, k_{1n3} is approximately linearly proportional to k_{2n}, and for large k_{1n3}, the excitation amplitude f is involved in the relationship. For different parameters, the new regression of the relation of the nonlinear coefficients k_{1n3} and k_{2n} modifies the design of the NL-VA.

For a case study, the nonlinear coefficient k_{1n3} of the primary system is set as $k_{1n3} = 150$ and the excitation amplitude is $f = 0.01$. From Fig. 6, the value of the nonlinear coefficient solved by Ref. [24] is $k_{2n} = 0.62$, which cannot realize the accurate Equal-peak effectiveness because of the strong nonlinearity. The designed k_{2n} obtained by Eq. (16) is $k_{2n} = 0.69$, which is larger than the value $k_{2n} = 0.62$ from Ref. [24]. A comparison of the amplitude-frequency curves for the nonlinear coefficient k_{2n} obtained in Ref. [24] and Eq. (16) is shown in Fig. 6.

From Fig. 6, for the designed nonlinear coefficient of NL-VA obtained by Eq. (16), the second peak is cut, and the two resonance peaks are forcibly equalized to each other. It is obvious that the k_{2n} obtained from the previous study (Ref. [24]) is insufficient for the Equal-peak and the De-nonlinearity properties because the second peak is higher than the first peak and the multi-steady states phenomenon exists. In addition, the comparison between HB1 and HB3 demonstrates that the solutions for only first harmonic and three harmonics are almost the same. In the following case studies and further applications, to guarantee the convergence and accuracy of the HBM solutions, especially for strong nonlinearity, the number of

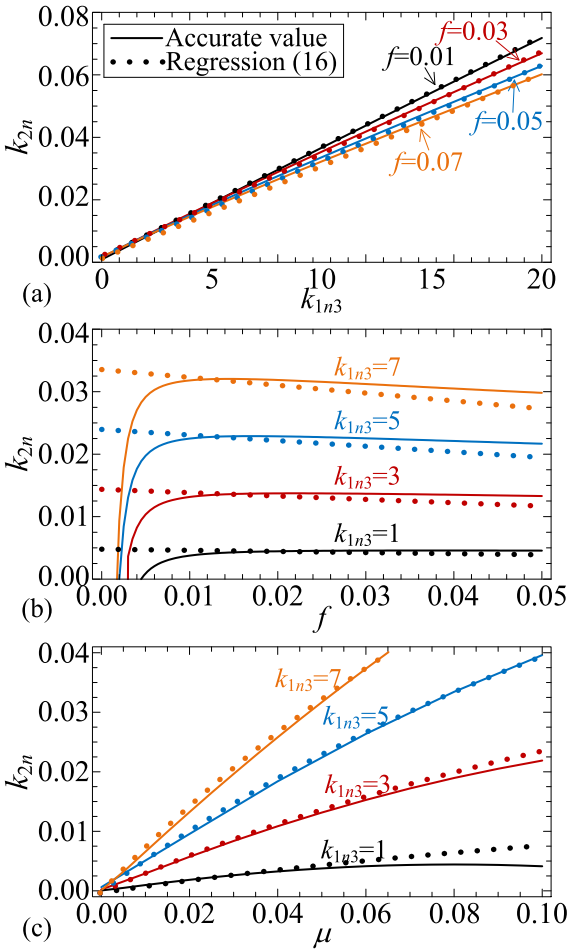

Fig. 5. The values of the designed nonlinear coefficient k_{2n} of NL-VA for (a) different k_{1n3}; (b) different f; (c) different μ.

harmonics is always chosen to be higher than the order of nonlinearity. Therefore, the proposed method can modify the accurate nonlinear design of the NL-VA for the Equal-peak and De-nonlinearity properties.

Next, we investigate the variations in multi-steady states bandwidth to show the effect and mechanism of the NL-VA on the De-nonlinearity property. For $k_{1n3} = 10$, we increase the nonlinear coefficient k_{2n} from zero. The multi-steady state bands and the amplitude-frequency curves are shown in Fig. 7 for different excitation amplitudes f.

As shown in Fig. 7, for different values of the excitation amplitude f, the values of k_{2n} for the Equal-peak property are very close because f has little effect on the proportion between k_{2n} and k_{1n3}, as indicated in the above section. However, for different f, the shapes of the amplitude-frequency curves are different. From the variation of multi-steady states band, each time we increase the excitation amplitude, the area of multi-steady states region increases because a larger f results the increase of response x_1, which in turn induces the multiply enhanced nonlinearity term $k_{1n3}x_1^3$. Also, since the solutions are obtained by perturbation method, for strong nonlinearity, from the Blue and Green curves in Fig. 7 (b), the value of k_{2n} obtained by the process as Fig. 4 has error for absolute accurate equal peak. Therefore, it is more difficult to eliminate the multi-steady states region effectively and the values of two resonance peaks have little error for larger f than k_{1n3}. When f is increased to approximately 0.035, the multi-steady state band is remarkably reduced but cannot be totally avoided for optimal k_{2n} by Eq. (16). Fortunately, as shown in Fig. 7 (b), regardless of the occurrence of multi-steady states and solution error from the perturbation method, the Equal-peak property can be realized for a wide range of the excitation amplitude f using the proposed modified method.

3.3.2. NL-VA on the primary system with seventh-order nonlinearity

The results and comparisons in the above case study revealed that the modified tuning method can obtain an accurate optimum nonlinear coefficient of the NL-VA for the Duffing nonlinear system. In recent years, research studies of novel nonlinear structures for vibration suppression have revealed that complex nonlinearity has advantages for vibration control,

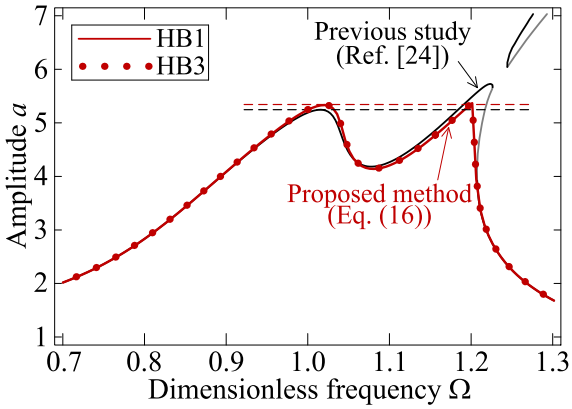

Fig. 6. Comparison of the amplitude-frequency curves for k_{2n} obtained by Ref. [24] (Black Lines) and by Eq. (16). The amplitude-frequency curves are solved by HB1 (Red Lines) and HB3 (Dots). (For interpretation of the references to colour in this figure legend, the reader is referred to the Web version of this article.)

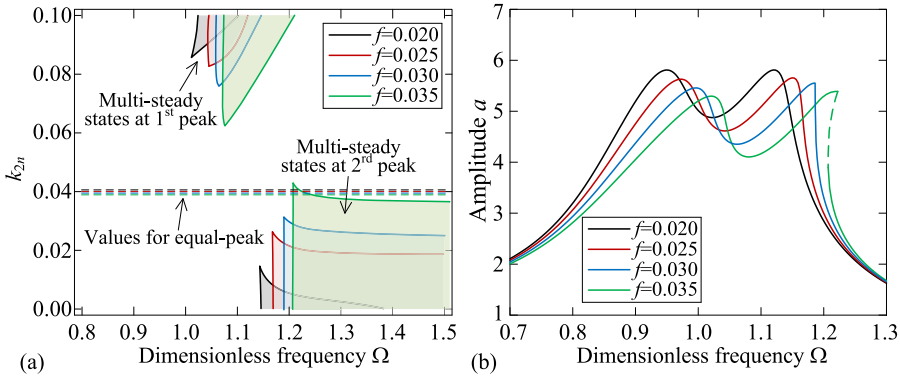

Fig. 7. (a) The multi-steady state bands for increasing k_{2n} and different f; (b) the amplitude-frequency curves for the Equal-peak property.

especially in the field for vibration isolation [1,2,5,31–34]. When the restoring force of the primary system is a complex nonlinear function [5,31–34], polynomial with multiple terms can describe the original nonlinearity more accurately than the Duffing nonlinearity. In Refs. [33,34], the seventh-order nonlinear function is utilized to fit the restoring force of the QZS vibration system. In this section, the availability of the proposed modified method for the NL primary system with seventh-order nonlinearity is investigated as a study case.

We follow the derivation process in Fig. 4 to design the nonlinear coefficient k_{2n} of the NL-VA for a NL primary system with multiple nonlinear terms. The seventh-order nonlinearity is considered as the case study. The dimensionless dynamical equation is written as

$$\begin{aligned} &x_1'' + x_1 + 2\xi_1 x_1' + \alpha_3 x_1^3 + \alpha_5 x_1^5 + \alpha_7 x_1^7 + \mu\gamma^2\widehat{x} + \mu\beta_3\widehat{x}_1^3 + 2\xi_2\mu\gamma\widehat{x}' = \cos(\Omega\tilde{t} + \phi_1), \\ &\widehat{x}'' + x_1 + 2\xi_1 x_1' + \alpha_3 x_1^3 + \alpha_5 x_1^5 + \alpha_7 x_1^7 \\ &\quad + (\mu+1)\gamma^2\widehat{x} + (\mu+1)\beta\widehat{x}_1^3 + 2(\mu+1)\xi_2\gamma\widehat{x}' = \cos(\Omega\tilde{t} + \phi_1), \end{aligned} \tag{17}$$

where $\alpha_3 = \frac{k_{1n3}}{k_{1l}}f^2$, $\alpha_5 = \frac{k_{1n5}}{k_{1l}}f^4$, $\alpha_7 = \frac{k_{1n7}}{k_{1l}}f^6$, $\beta = \frac{k_{2n}}{M_2\omega_1^2}f^2$, and the other dimensionless parameters are the same as those in Eq. (3). In this case study, because the highest nonlinearity is seventh-order, the solution is set with more than seven harmonics for convergence and accuracy.

The linear coefficients of primary system are set as $M_1 = 1$, $k_{1l} = 1$, and $c_1 = 0.002$, and the nonlinear coefficients are set as $k_{1n3} = 1\ \mathrm{N\,m^{-3}}$, $k_{1n5} = 1\times10^4\ \mathrm{N\,m^{-5}}$, and $k_{1n7} = 1\times10^5\ \mathrm{N\,m^{-7}}$. For the excitation amplitude $f = 0.01$, the amplitude-frequency curves of the primary system with the designed k_{2n} determined by the previous study in Ref. [24] (considering only k_{1n3}) and the modified method (considering all nonlinear coefficients) are shown in Fig. 8 for comparison. In Fig. 8, the black line represents the amplitude-frequency curve when $k_{2n} = \frac{2\mu^2}{1+4\mu}\ k_{1n3} = 0.0042\ \mathrm{N\cdot m^{-3}}$, as given in Ref. [24], and the red line

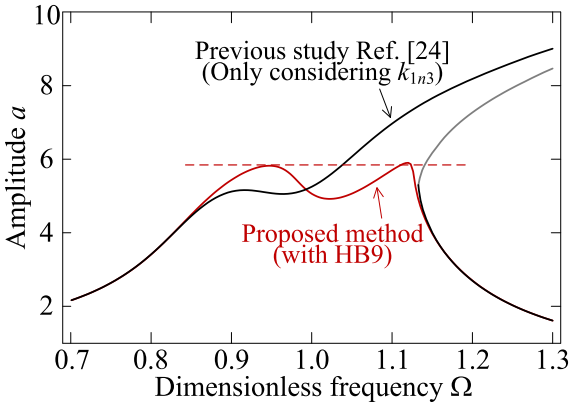

Fig. 8. Comparison of the amplitude-frequency curves of the primary system between the value of k_{2n} only considering k_{1n3} and that considering all nonlinear coefficients.

represents the amplitude-frequency when $k_{2n} = 0.124\ \mathrm{N\,m^{-3}}$ with the consideration of all terms of nonlinearity by assuming the solution with the first harmonic to the ninth harmonic.

From the comparison in Fig. 8, it is obvious that the designed k_{2n} by the proposed method realizes the Equal-peak and De-nonlinearity properties effectively. This result reveals that the value of k_{2n} with consideration of only k_{1n3} is much smaller than the value obtained with the consideration of all nonlinear terms. Thus, this result verifies that the proposed modified method can determine the optimum nonlinear coefficient of the NL-VA for the primary vibration system with complex nonlinearity.

The effect of k_{2n} on the De-nonlinearity property for increasing excitation amplitude f and nonlinear strength k_{1nj} ($j = 3,5,7$) is investigated. For different f and k_{1nj}, the multi-steady state bands and amplitude-frequency curves for the critical values and optimal values of k_{2n} are revealed in Fig. 9.

From Fig. 9, when a large nonlinearity of the primary system or excitation amplitude induces the multi-steady states band, the increase of the k_{2n} of NL-VA can effectively change its bandwidth. Because of the multiple nonlinear terms, the variation in the multi-steady states band is different from the first case for the Duffing primary system. To increase k_{2n} from zero to a specific value, the amplitude-frequency curve at the multi-steady states band is divided. With the further increase of k_{2n}, the upper curve increases and the lower curve decreases. The critical point for the division of the amplitude-frequency curve is defined as the Breakpoint in Fig. 9 (a) and (d). When k_{2n} is fixed at the breakpoint, the amplitude-frequency curves are cut at the frequency of the breakpoint, as shown in Fig. 9 (b) and (e). When the second resonance peak on the lower amplitude-frequency curve is higher than the first one as the k_{2n} reaches the breakpoint value, with the increase of k_{2n} to the equal-peak value, the second resonance peak is depressed and the accurate Equal-peak property can be realized. To the contrary, at the breakpoint of k_{2n}, the second resonance peak is lower than the first one, then, with the increase of k_{2n} till the Equal-peak value, the second resonance peak is further decreased and is lower than the first one (as the Blue line shown in Fig. 9 (f)). The reason for the inaccurate Equal-peak property is induced by the strong nonlinearity and the conditions of equal peak lose the efficiency. Also, at the value of k_{2n} for the Equal-peak property, the upper and lower curves have divided at far distances; thus, the De-nonlinearity property is also achieved with the mechanism of local bifurcation introduced by the nonlinearity. Therefore, the Equal-peak method can be explored in a primary system with complex nonlinearity using the proposed derivation process.

3.3.3. NL-VA on the primary system with QZS nonlinearity

For a primary system with QZS property, based on its structural design, its resonance frequency can be reduced to nearly zero for the High-Static-Low-Dynamic property. From the modelling in Refs. [1,2,5,29–34], it is known that the expression of the restoring force of the vibration system with QZS property is an irrational function. Although some previous studies [2,5,29] utilize a third-order Taylor series expansion to describe the irrational stiffness function around the zero equilibrium, there exists an obvious error between the expansion and the original function for large motion [1,30–34]. Because a significant QZS system should be applicable for low-frequency and large-amplitude excitation, there usually is a high resonance peak at the low-frequency band and the multiple-terms nonlinearity should be considered in this investigation. As QZS structure is utilized as elastic component from the primary mass to the base, the excitation cannot be isolated in the resonance frequency bands. Therefore, when the primary system has QZS property, to suppress the vibration and eliminate the nonlinear performances at the resonance frequency band, NL-VA is designed according to the proposed processing. The configuration of the primary system with QZS property coupled NL-VA is shown in Fig. 10.

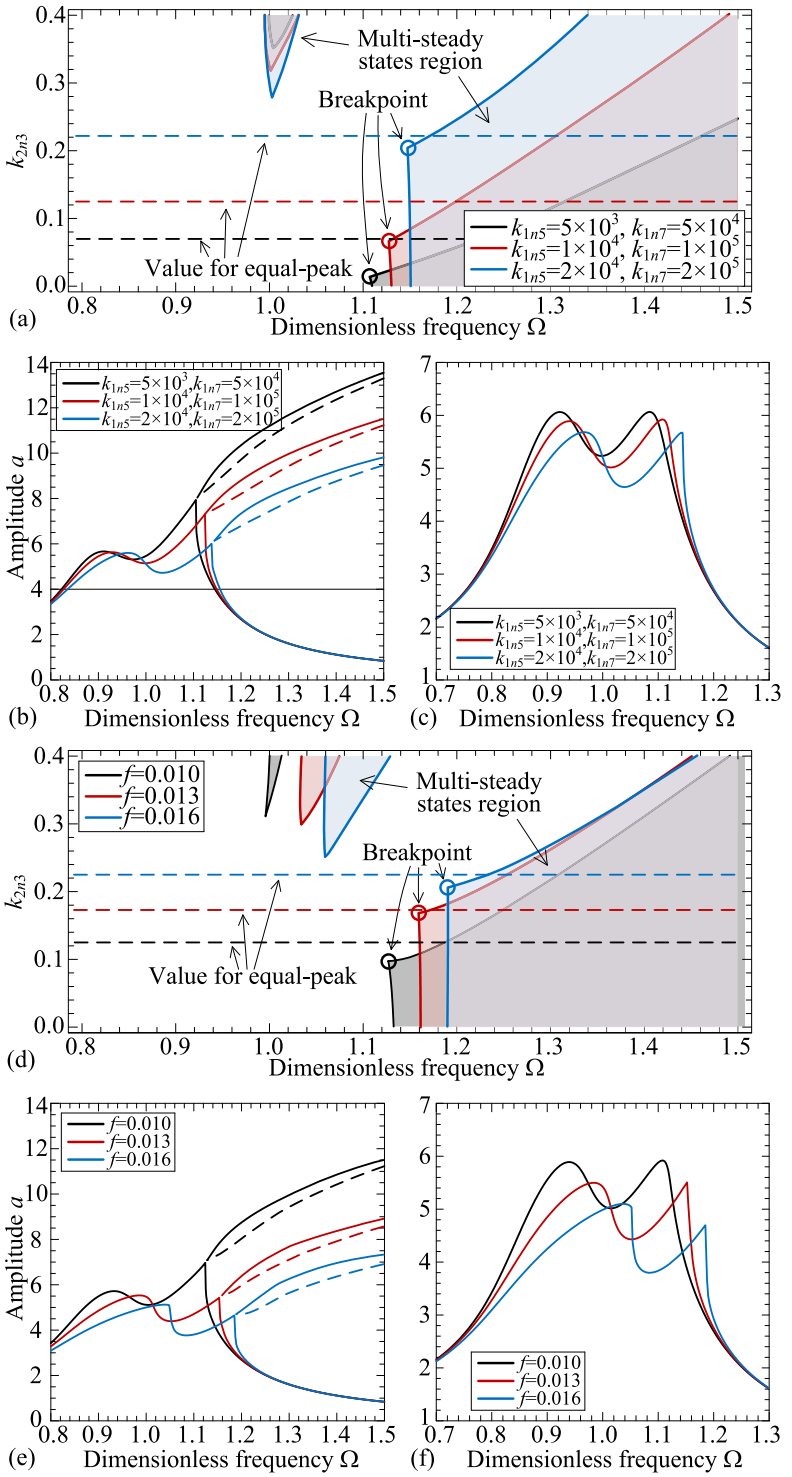

Fig. 9. (a) Multi-steady states bands for increasing k_{1n5} and k_{1n7} when $f = 0.01$; (b) the amplitude-frequency curves when k_{2n} is chosen at the breakpoint; (c) the amplitude-frequency curves for the Equal-peak property; (d) multi-steady state bands for increasing excitation amplitude f; (e) the amplitude-frequency curves when k_{2n} is chosen at the breakpoint; (f) the amplitude-frequency curves for the Equal-Peak property.

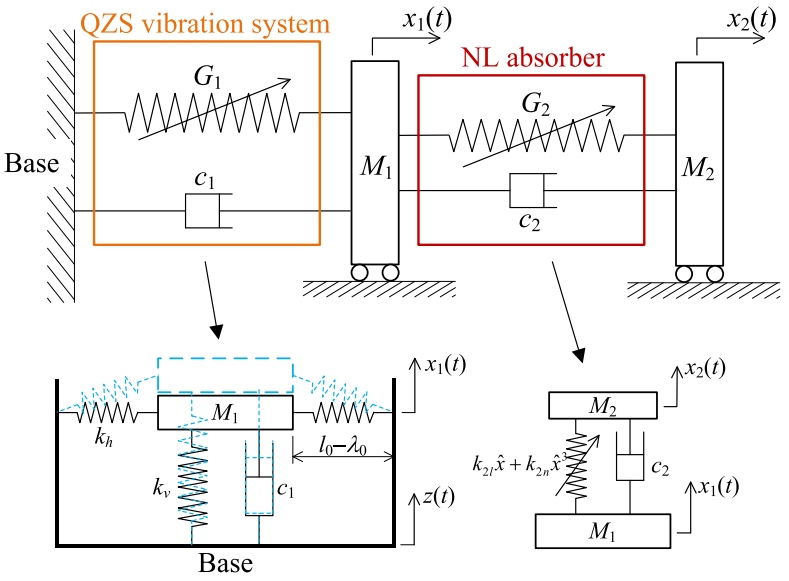

Fig. 10. The structural configuration of the primary system with QZS property coupled a NL-VA.

As shown in Fig. 10, we consider the primary system with QZS property as Refs. [1,2,5,29–34]. According to Ref. [34], the restoring force of the primary system has multiple nonlinear terms, defined as $G_1(\hat{x}_1)$ where $\hat{x}_1 = x_1 - z$. The restoring force of the NL-VA is still given as $k_{2l}(\cdot) + k_{2n}(\cdot)^3$. The dynamical equation is written as

$$\begin{aligned} &M_1\ddot{\hat{x}}_1 + G_1(\hat{x}_1) + c_1\dot{\hat{x}}_1 + k_{2l}\hat{x} + k_{2n}\hat{x}^3 + c_2\dot{\hat{x}} = M_1\ddot{z}, \\ &M_2\ddot{\hat{x}} + \mu G_1(\hat{x}_1) + \mu c_1\dot{x}_1 + (\mu+1)\left(k_{2l}\hat{x} + k_{2n}\hat{x}^3\right) + (\mu+1)c_2\dot{\hat{x}} = \mu M_1\ddot{z}. \end{aligned} \tag{18}$$

where $\hat{x} = x_1 - x_2$ and z is the base excitation as $z = z_e\cos(\omega t + \phi_1)$. According to the investigations in Refs. [1,2,5,29–34] and the deformations of the elastic components in the QZS primary system shown in Fig. 10, the restoring forces G_1 are written as

$$G_1(\hat{x}_1) = k_v\hat{x}_1 + 2k_h\hat{x}_1\left(1 - \frac{l_0}{\sqrt{(l_0-\lambda_0)+\hat{x}_1^2}}\right). \tag{19}$$

In Eq. (19), the restoring force G_1 is an irrational symmetrical function that satisfies $G_1(0) = 0$. We utilize the polynomial function g_1 to describe G_1 to simplify the analysis rather than using the third-order Taylor series expansion. To apply the primary system for large excitation, we consider a polynomial function g_1 with $(2i+1)$ order, written as

$$g_1(\hat{x}_1) = k_v\hat{x}_1 + g_{n1}(\hat{x}_1) = k_{1l}\hat{x}_1 + \sum_{i=1}^{n} k_{1n(2i+1)}\hat{x}_1^{2i+1}. \tag{20}$$

where $k_{1n(2i+1)}$ $(i = 1,2,\ldots,n)$ is the fitting nonlinear coefficient, which is obtained by the least square method (LSM). The processing is listed in Appendix C. For the same term number for the polynomial and Taylor series expansion, the comparison is shown in Fig. C.1. From the comparison in Fig. C.1, the restoring force of the primary system with QZS property can be accurately described by a fitting polynomial with multiple terms rather than Taylor series expansion. When the dimensionless motion $\hat{x}_1$ is raised and close to 1, the difference between the Taylor series expansion and the original function dramatically increased. Thus, the fitting polynomial is required to describe the original irrational function accurately.

Referring to the dimensionless transformation given by Eq. (3), the dimensionless parameter transformation introduced is given by

$$
\begin{aligned}
&k_\gamma = \frac{k_h}{k_v}, \lambda_s = \frac{\lambda_0}{l_0}, \omega_1 = \sqrt{\frac{k_{1l}}{M_1}}, \tilde{t} = \omega_1 t, \alpha_{2i+1} = \frac{k_{1n(2i+1)}}{k_{1l}},\\
&\omega_2 = \sqrt{\frac{k_{2l}}{M_2}}, \gamma = \frac{\omega_2}{\omega_1}, 2\xi_1 = \frac{c_1}{M_1\omega_1}, 2\xi_2 = \frac{c_2}{M_2\omega_2},\\
&\beta = \frac{k_{2n}}{M_2\omega_1^2} z_e^2 = \frac{k_{2n}}{\mu k_{1l}} z_e^2, \Omega = \frac{\omega}{\omega_1}.
\end{aligned}
\tag{21}
$$

In the parameter transformation Eq. (21), k_γ reflects the stiffness ratio of the vertical and horizontal springs in the QZS system; λ_s is the ratio between the pre-deformation length and the original length of the horizontal spring, the value of which should in the range of [0, 1]. The dimensionless dynamical equation is written as

$$
\begin{aligned}
&\widehat{x}_1'' + \widehat{x}_1 + \sum_{i=1}^{n} \alpha_{2i+1}\widehat{x}_1^{2i+1} + 2\xi_1\widehat{x}_1' + \mu\gamma^2\widehat{x} + \mu\beta\widehat{x}^3 + 2\xi_2\mu\gamma\widehat{x}' = \Omega^2\cos(\Omega\tilde{t} + \phi_1),\\
&\widehat{x}'' + \widehat{x}_1 + \sum_{i=1}^{n} \alpha_{2i+1}\widehat{x}_1^{2i+1} + 2\xi_1\widehat{x}_1'\\
&\quad +(\mu+1)\gamma^2\widehat{x} + (\mu+1)\beta\widehat{x}^3 + 2\xi_2(\mu+1)\gamma\widehat{x}' = \Omega^2\cos(\Omega\tilde{t} + \phi_1).
\end{aligned}
\tag{22}
$$

Next, the functions H_1 and H_2 are obtained by solving Eq. (22) via HBM. Setting the structural parameters of the primary system as $M_1 = 1$, $k_v = 1$, $k_\gamma = k_h/k_v = 0.5$ and $c_1 = 0.002$, the parameters of the linear parts M_2, k_{2l} and c_2 of the NL-VA are designed according to the pervious study as Eq. (5). For $\mu = 0.05$, $k_{2l} = 0.04535k_{1l}$, $c_2 = 0.012756\sqrt{k_{1l}}$ and the nonlinear parameter k_{2n} of NL-VA are determined using the proposed method based on the process shown in Fig. 4. For different pre-deformation ratios λ_s, the fitting polynomial functions g_1 for the restoring force of the primary system with multiple nonlinear terms are shown in Table 1 in Appendix D. The values of the nonlinear parameter k_{2n} of NL-VA with increasing z_e and λ_s are shown in Fig. 11.

For the realization of the Equal-peak and De-nonlinearity properties of the nonlinear primary system with multiple nonlinear terms, the optimum values of the nonlinear coefficient k_{2n} of NL-VA depend on both structural parameters and excitation parameters. From the expressions of g_1 shown in Table 1 in Appendix D, for increasing the pre-deformation ratio λ_s, the fifth-order nonlinear coefficients negatively increase, and thus the nonlinearity weakens with larger λ_s. As a result, for smaller λ_s, the nonlinear coefficient k_{2n} becomes much more different for different excitation amplitudes z_e. For larger λ_s, the values of k_{2n} tend to approach each other. From Fig. 11, for a NL primary system with multiple nonlinear terms, we obtain the nonlinear coefficient of NL-VA to realize the Equal-peak and De-nonlinearity properties. For different values of z_e and λ_s, the amplitude-frequency curves are shown in Fig. 12.

Fig. 12 shows the effect of NL-VA on the vibration responses of the primary system with multiple nonlinear terms in the frequency domain. Fig. 12 (a) shows that utilizing L-VA cannot suppress the amplitude of the primary system around the second resonance frequency and avoid the multi-steady states phenomenon; furthermore, when utilizing the NL-VA with the designed nonlinear coefficient k_{2n}, the adverse nonlinear vibration performances are avoided by the realization of both Equal-peak and De-nonlinearity properties. From the results in the frequency domain, we can conclude that for a primary system with multiple nonlinear terms, the static capacity can be guaranteed because M_2 is much smaller than M_1; moreover, the

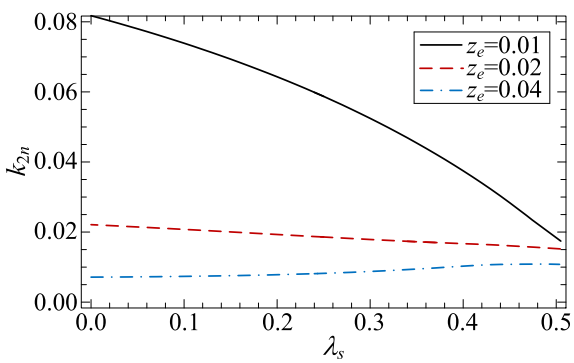

Fig. 11. The nonlinear coefficient k_{2n} of the NL-VA for increasing base excitation amplitudes on the primary system with multiple nonlinear terms for increasing λ_s.

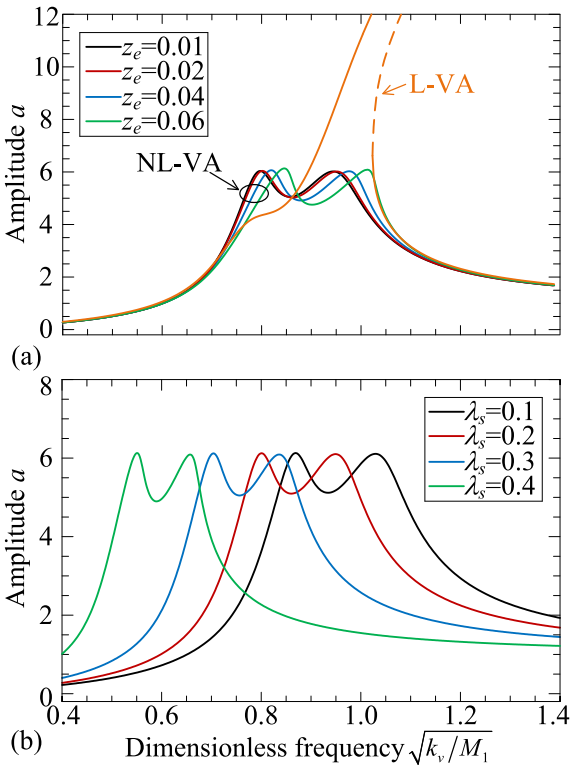

Fig. 12. The amplitude-frequency curves (a) for different base excitation amplitudes z_e when $\lambda_s = 0.2$ and (b) for different pre-deformations λ_s when $z_e = 0.02$.

effective frequency band for vibration suppression can be widened to the low-frequency band by increasing λ_s without the possibility of multi-steady states being induced by the increase of nonlinearity. Therefore, using the proposed modified method, the NL-VA with an optimum design is significantly beneficial for the dynamical vibration performance of the primary system with QZS property.

In conclusion, based on the case studies of primary systems with different multiple nonlinear terms, especially for the vibration systems with QZS property [1,2,5,29–34], the results of the vibration performances on the frequency domain verify the significant effect of the modified design method of the nonlinear NL-VA. By applying an optimum-designed NL-VA, the resonance peak at low-frequency band can be suppressed, and thus the dynamical bifurcations [20,32] can be avoided.

4. The verification experiments of VAs with linear and nonlinear properties

4.1. The construction of the system with VA

The experimental construction of the system consisted of the nonlinear primary system and vibration absorber is shown in Fig. 13. The primary system vibrates under the excitation from the base and the VA is applied on the primary system. In the experiment, the laser is utilized to measure the vibration of the primary system.

As shown in Fig. 13, the restoring force of the primary system is nonlinear and the restoring force of the VA depends on its structure, which is designed according to the proposed method.

In experiments, the prototype of primary system is constructed as shown in Ref. [34], which has QZS property for induce high-static-low-frequency in some specific fields [1,2]. The experimental construction and deformation are shown in Appendix D. This kind of vibration system has multiple-nonlinear terms and quasi-zero linear stiffness coefficient, and thus, it has a high resonance peak at low frequency band and obvious nonlinear multi-steady state phenomenon. On the primary system, L-VA and NL-VA are applied to suppress the vibration of the NL primary system in resonance frequency band. Referring [34], dimensionless dynamical equation of the primary system is written as

$$\ddot{\hat{x}}_1 + \omega_1^2 \hat{x}_1 + \sum_{j=1}^{n} \alpha_{2j+1} \hat{x}_1^{2j+1} + \xi_1 \dot{\hat{x}}_1 = -\ddot{z}. \tag{23}$$

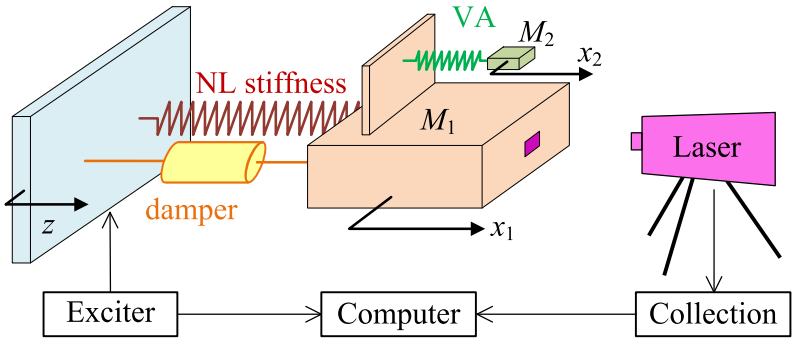

Fig. 13. The construction of the system with primary system and VA.

According to the restoring force property of the vibration system as Ref. [34], the restoring force can be approximately described by polynomial with multiple terms as Eq. (23). In Eq. (23), ω_1 is the natural frequency, α_{2j+1} the nonlinear coefficient and ξ_1 is the damping coefficient.

4.2. The coefficients of the primary system by identification

Firstly, the coefficients of the primary system are identified without the VA. In identification experiment, the excitation is harmonic vibration as $z = z_e\cos(\omega t+\phi_1)$ and the response of the primary system $\widehat{x}_1$ as $\widehat{x}_1 = a\cos\omega t$. In the experiment, for discrete excitation frequencies $\omega_k\,(k = 1,2,\ldots,m)$, the point-by-point response amplitudes of the primary system measured are a_k. Based on the least square method (LSM), the error between the response amplitude solved by Eq. (23) and the measured ones should be minimized. Thus, the parameters should satisfy the following equation systems:

$$\frac{\partial}{\partial \boldsymbol{\chi}}\sum_{k=1}^{m}[W(a_k,\omega_k)]^2 = 0, \tag{24}$$

where $\boldsymbol{\chi}$ represents the parameters to be identified for $\boldsymbol{\chi} = \{\omega_1, \xi_1, \alpha_{2j+1}\}^T$. The coefficients of the NL primary system are listed in Table 2. Also, Fig. 14 shows the point-by-point amplitudes for different excitation frequencies obtained by dynamical equation as $j = 5$ with parameters by identification and the obtained by experiments.

From Fig. 14, the amplitude-frequency curve verifies obvious nonlinearity of the primary system. For the identification results, as $\omega = 4$ Hz, two amplitudes are obtained. Thus, the primary system is nonlinear although it is too difficult to see the multi-steady states phenomenon in experiment. In addition, the results in Fig. 14 shows the dynamical performances and resonance peak of the primary system without the VA measured in experiment.

4.3. Experimental prototypes for L-VA and NL-VAs

4.3.1. The construction of L-VA and NL-VAs

In the experiment, we construct VAs to realize the Equal-peak and De-nonlinearity properties for the NL primary system. To verify the proposed design method for the VA, a L-VA and two NL-VAs are respectively assembled on the nonlinear primary system, and then their vibration performances for vibration absorption are compared. The constructions and mechanical models of the proposed L-VA and NL-VAs are shown in Fig. 15. Because the restoring forces of L-VA and NL-VAs are different, the elastic components and constructions of L-VA and NL-VA are completely different. The L-VA is realized by an elastic beam and two NL-VAs with different structural parameters are realized by elastic origami mechanism [35,36].

As shown in Fig. 15(a) and (b), the restoring force of the L-VA is as a lightweight elastic cantilever beam. The mass M_2 is concentrated at the free end of the cantilever beam. Thus, the dynamical equation of the designed L-VA shown in Fig. 15(a) and (b) is written as

Table 2
The coefficients of the NL primary system by identification for $j = 5$.

ω_1 (rad/s)	ω_1 (Hz)	ξ_1	γ_3	γ_5	γ_7	γ_9	γ_{11}
23.419	3.72	0.0047	62394	382742.5	4.075×10^8	3.7×10^{10}	3.42×10^{12}

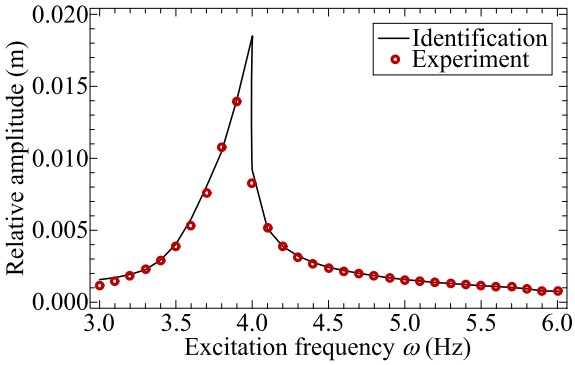

Fig. 14. Amplitude-frequency curves for identification (Lines) and amplitudes from experiments (Dots).

$$M_2\ddot{x}_2 + k_{2l}x_2 + c_2\dot{x}_2 = u(t). \tag{25}$$

where k_{2l} is the stiffness of the transverse vibration of the cantilever beam.

On the other hand, we explore the Origami mechanism [36] to realize the adjustable nonlinearity of the NL-VA due to geometrical nonlinearity. In the NL-VAs, ρ_i ($i = 1,2, \ldots,6$) reflects the fold with original angle φ_{i0}. Based on the analysis of the Origami structure [35,36], the restoring force is a tunable nonlinear function for different assembly angles. The dynamical equation of the NL-VA is written as

$$M_2\ddot{x}_2 + k_{2l}x_2 + k_{2n}x_2^3 + c_2\dot{x}_2 = u(t). \tag{26}$$

where k_{2l}, k_{2n} and c_2 can be adjusted by the different structural parameters of the Origami structure.

4.3.2. The coefficients of the NL-VAs by identification

When the coefficients of the NL primary system are fixed as Table 2, the nonlinearity of VA should be designed to realize Equal-peak and De-nonlinearity properties. In the experiment, the mass of absorber M_2 is much smaller than M_1 and is designed as $M_2 = \mu M_1 = 0.055 \times M_1 \approx 0.025$ kg. Then, the optimum linear coefficients of L-VA are designed according to Eq. (5) as Ref. [24] as $k_{2l} \approx 12.44\ \mathrm{N\,m^{-1}}$, $c_2 \approx 0.14\ \mathrm{N\,s\,m^{-1}}$; the optimum nonlinear coefficients of NL-VAs are determined by the process of proposed method shown in Fig. 4, approximately as $k_{2n} \approx 1017.47\ \mathrm{N\,m^{-3}}$ for $z_e = 0.3$ mm.

In the L-VA, the cross section and length of beam determine the stiffness. In the NL-VA by Origami structure, to induce the required natural frequency and Duffing nonlinearity, two structural parameters, namely, the length of plane l_f and original angle of fold φ_{10}, are changed. For smaller l_f, the natural frequency increases, whereas for smaller φ_{10}, the natural frequency decreases. Based on the design of structural parameters, the L-VA, NL-VA-1 and NL-VA-2 have nearly equal linear stiffness coefficient. The parameters of the L-VA, NL-VA-1 and NL-VA-2 are identified by respective experiments, as shown in Fig. 16.

From the identification results and comparison in Fig. 16, it can be seen that the NL-VA-1 and NL-VA-2 reveal nonlinear vibration performance because its resonance frequency offsets to a high frequency value. Also, the nonlinearity strength of the NL-VA-2 is stronger than NL-VA-2. The values of the identification parameters are listed in Table 3.

As shown in Table 3, from the identification results, the linear coefficient of L-VA is very close to the optimum design value while the linear coefficients of the two NL-VAs have little deviation from the optimum value. The nonlinear stiffness coefficient k_{2n} for NL-VA-1 and NL-VA-2 is both larger than the optimum value $k_{2n} \approx 1017.47\ \mathrm{N\,m^{-3}}$. In addition, compared the nonlinear coefficients of NL-VA-1 and NL-VA-2, the strength of nonlinearity of NL-VA-2 is larger than NL-VA-1 due to its angle of fold is larger than NL-VA-1 [36].

4.4. The effectiveness of the designed L-VA and NL-VAs

We assemble the L-VA, NL-VA-1 and NL-VA-2 on the nonlinear primary system and measure the responses of M_1 for the three cases separately. The amplitude of base excitation is fixed at $z_e = 0.3$ mm, and the excitation frequency varies from 2.5 Hz to 5 Hz with an interval of 0.1 Hz. The absolute motion amplitudes of the primary system are measured as shown in Fig. 17.

Fig. 17 demonstrates that VA can reduce the resonance of the primary system and the nonlinearity of VA is beneficial for the vibration suppression compared to the effect of the L-VA. For L-VA, since its linear stiffness $k_{2l} = 12.71$ is very close to the optimum $k_{2l} = 12.44$, there is an anti-frequency band around 3.7 Hz, where is the original resonance peak of the primary

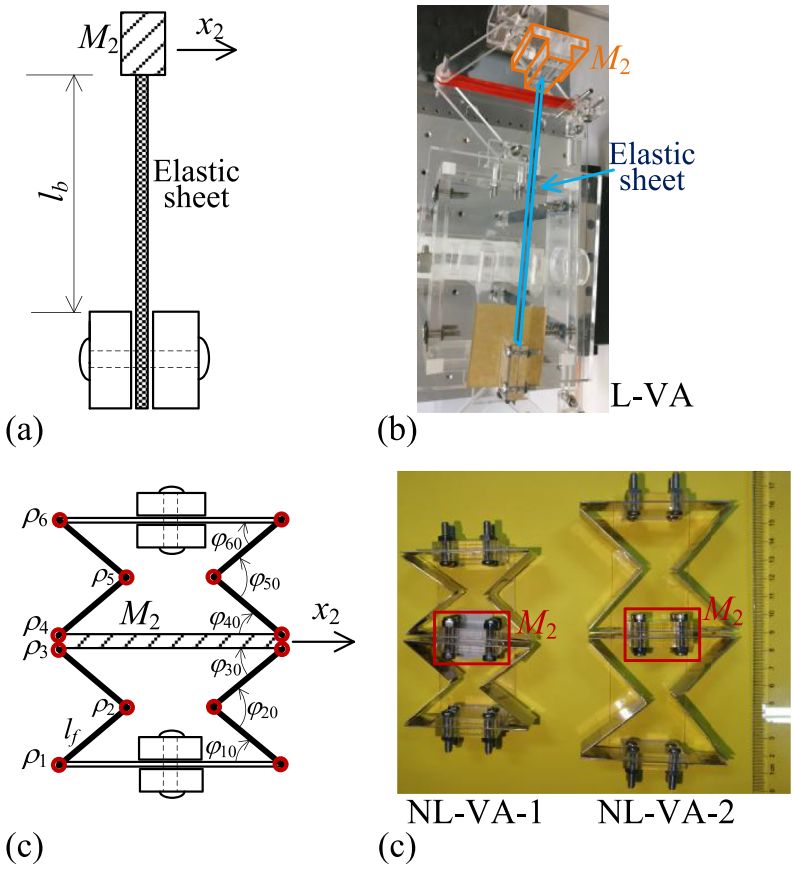

Fig. 15. (a) The mechanical model of L-VA, (b) the experimental prototype for L-VA; (c) the mechanical model of NL-VA, (d) two experimental prototypes for NL-VAs.

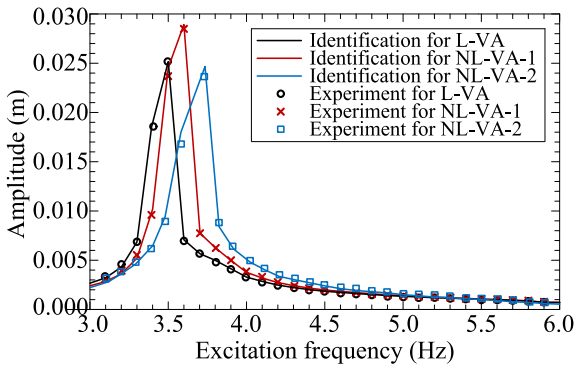

Fig. 16. Identification results of the L-VA, NL-VA-1 and NL-VA-2 compared with the experimental measurement for different excitation frequencies.

system (about 3.7 Hz in the definition results as shown in Fig. 14 and Table 2). However, the two resonance peaks of the primary system with L-VA are unequal and the amplitude around the second resonance is very high since the nonlinear coefficient of the L-VA equals to zero. For NL-VAs, the second resonance peak is significantly reduced by increasing the nonlinearity. It can be seen that by respectively applying NL-VA-1 and NL-VA-2 on primary system, the vibration performances at two resonance bands are tuned. For NL-VA-1, the two resonance peaks are controlled at a low value, and their values are close. The second resonance peak is lower than the first resonance peak because the actual value of k_{2n} of the NL-VA utilized is $k_{2n} \approx 1233\ \mathrm{N\,m^{-3}}$, which is little larger than the designed value of $k_{2n} \approx 1017\ \mathrm{N\,m^{-3}}$. On the other hand, for NL-VA-2, which has much greater nonlinearity than the NL-VA-1, the second resonance peak is further reduced since the nonlinear

Table 3
The structural parameters and identified coefficients of the L-VA, NL-VA-1 and NL-VA-2.

	φ_{10}	l_f	M_2	μ	k_{2l}	$\gamma=\omega_2/\omega_1$	c_2	k_{2n}
optimum				0.55	≈12.44	1	≈0.14	≈1017.47
L-VA			0.027	0.054	12.71	0.927	0.164	
NL-VA-1	40°	3 mm	0.029	0.058	14.16	0.91	0.1922	1233.75
NL-VA-2	50°	5 mm	0.029	0.058	14.21	0.91	0.2179	3427.08

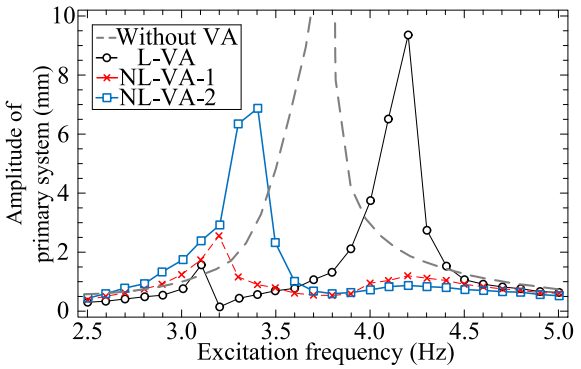

Fig. 17. The amplitudes of the primary system in frequency domain for the cases without VA (Dashed lines), L-VA ("○"), NL-VA-1 (" × ") and NL-VA-2 ("□") by experiments.

coefficient of NL-VA-2 is $k_{2n}=3427.08$. The two resonance peaks for NL-VA-1 and NL-VA-2 prove that the nonlinearity can effectively adjust the magnitude of the two resonance peaks. Also, the variations of the two resonance peaks conform to the theoretical analysis and the effect of nonlinearity in NL-VA is verified. Therefore, the experimental results verify the benefits introduced by the nonlinearity on the Equal-peak and De-nonlinearity properties. In addition, for the NL-VA, its mass is much lower than that of the primary system, and the machine size is very small; these characteristics can potentially be of use in engineering practices.

5. Conclusions

In this paper, we explored the nonlinear tuning method of NL-VA for primary system with multiple nonlinear stiffness terms under force/base excitation. The nonlinearity of NL-VA was designed to suppress the nonlinear resonance vibration in resonance frequency band. The vibration performances and control mechanism were investigated both theoretically and experimentally. The following conclusions can be drawn based on our results and discussions.

(a) This study proposed a generalized method to determine the optimal values of nonlinear coefficient of NL-VA by high-order harmonic analysis. Because the expressions of resonance frequencies and solution of steady states are obtained theoretically, the optimal nonlinear coefficient of NL-VA for equal-peak is determined accurately for different excitation amplitudes over a very wide range;
(b) Based on the theoretical results, is finds that utilizing NL-VA on the nonlinear primary system not only reduces the resonance peaks but also eliminates undesirable nonlinear vibration performances, such as multi-steady states. According to local bifurcation analysis, the relation between the bandwidth of multi-steady states and nonlinear coefficient of NL-VA is established. It is found that applying nonlinearity to a nonlinear primary system can realize the De-nonlinearity property;
(c) Since it has discovered that the large response at the resonance can be suppressed, the vibration performances at the resonance band of the nonlinear primary system with QZS property can be improved without changing any components of it;
(d) A novel experimental prototype of the NL-VA system was realized via an Origami structure. The nonlinear coefficient of the NL-VA can be adjusted by changing the structural parameters. The comparison of the amplitude-frequency curves of the primary system among L-VA, NL-VA-1 and NL-VA-2 verifies the effect of nonlinearity of VA on Equal-peak and De-nonlinear properties. This study revealed an innovative use of the Origami mechanism in the field of vibration control to provide adjustable dynamical nonlinearity.

In conclusion, the optimum design of NL-VA according to the modified nonlinear tuning method can realize both Equal-peak and De-nonlinearity properties, both of which have significantly potential applications in low-frequency nonlinear vibration systems such as ships and aircrafts.

Acknowledgements

The authors would like to gratefully acknowledge the support from the National Natural Science Foundation of China under Grant No. 11772229 and No. 11602141, the Shanghai Sailing Program No. 16YF1408000, and the Natural Science Foundation of Shanghai No. 16ZR1423600.

Appendix A

Substituting $\widehat{x} = x_1 - x_2$ into Eq. (1), the dynamical equation is written as

$$\begin{aligned} &M_1\ddot{x}_1 + G_1(x_1) + c_1\dot{x}_1 + G_2(\widehat{x}) + c_2\dot{\widehat{x}} = u(t), \\ &M_2\left(\ddot{x}_1 - \ddot{\widehat{x}}\right) - G_2(\widehat{x}) - c_2\dot{\widehat{x}} = 0. \end{aligned} \tag{A.1}$$

Re-arranging the second equation in (A.1) by substituting $\ddot{x}_1 = \frac{1}{M_1}[-G_1(x_1) - c_1\dot{x}_1 - G_2(\widehat{x}) - c_2\dot{\widehat{x}} + u(t)]$ into it, (A.1) is given as

$$\begin{aligned} &M_1\ddot{x}_1 + G_1(x_1) + c_1\dot{x}_1 + G_2(\widehat{x}) + c_2\dot{\widehat{x}} = u(t), \\ &M_2\ddot{\widehat{x}} + G_2(\widehat{x}) + c_2\dot{\widehat{x}} = M_2\ddot{x}_1 = \frac{M_2}{M_1}\left[- G_1(x_1) - c_1\dot{x}_1 - G_2(\widehat{x}) - c_2\dot{\widehat{x}} + u(t)\right]. \end{aligned} \tag{A.2}$$

Introducing the parametrical transformation of $\mu = \frac{M_2}{M_1}$, the dynamical equation can be written as

$$\begin{aligned} &M_1\ddot{x}_1 + G_1(x_1) + c_1\dot{x}_1 + G_2(\widehat{x}) + c_2\dot{\widehat{x}} = u(t), \\ &M_2\ddot{\widehat{x}} + \mu G_1(x_1) + \mu c_1\dot{x}_1 + (\mu+1)G_2(\widehat{x}) + (\mu+1)c_2\dot{\widehat{x}} = \mu u(t). \end{aligned} \tag{A.3}$$

Next, further introducing simplification as $k_{1n} = \frac{\mathrm{d}^3 G_1}{\mathrm{d}x_1^3}\Big|_{x_1=0}$ and $k_{2n} = \frac{\mathrm{d}^3 G_2}{\mathrm{d}\widehat{x}^3}\Big|_{\widehat{x}=0}$, Eq. (A.3) can be simplified to Eq. (2).

Substituting the parametrical dimensionless transformation given by Eq. (3) into Eq. (2), the following equations can be obtained:

$$\begin{aligned} &M_1\frac{k_{1l}}{M_1}x_1'' + k_{1l}x_1 + k_{1n}x_1^3 + c_1\sqrt{\frac{k_{1l}}{M_1}}x_1' + k_{2l}\widehat{x} + k_{2n}\widehat{x}^3 + c_2\sqrt{\frac{k_{1l}}{M_1}}\widehat{x}' = f\cos\left(\omega_1\Omega\cdot\frac{\tilde{t}}{\omega_1}\right), \\ &M_2\frac{k_{1l}}{M_1}\widehat{x}'' + \mu k_{1l}x_1 + \mu c_1\sqrt{\frac{k_{1l}}{M_1}}x_1' + \mu k_{1n}x_1^3 \\ &+ (\mu+1)k_{2l}\widehat{x} + (\mu+1)k_{2n}\widehat{x}^3 + (\mu+1)c_2\sqrt{\frac{k_{1l}}{M_1}}\widehat{x}' = \mu f\cos\left(\omega_1\Omega\cdot\frac{\tilde{t}}{\omega_1}\right), \end{aligned} \tag{A.4}$$

We re-arrange the above equation as

$$\begin{aligned} &x_1'' + x_1 + \frac{k_{1n}}{k_{1l}}x_1^3 + c_1\frac{1}{\sqrt{M_1k_{1l}}}x_1' + \frac{k_{2l}}{k_{1l}}\widehat{x} + \frac{k_{2n}}{k_{1l}}\widehat{x}^3 + c_2\frac{1}{\sqrt{M_1k_{1l}}}\widehat{x}' = \frac{f}{k_{1l}}\cos(\Omega\tilde{t}), \\ &\widehat{x}'' + \frac{M_1}{M_2}\mu x_1 + \frac{M_1}{M_2}\mu c_1\frac{1}{\sqrt{M_1k_{1l}}}x_1' + \frac{M_1}{M_2}\mu\frac{k_{1n}}{k_{1l}}x_1^3 + (\mu+1)\frac{M_1}{M_2}\frac{k_{2l}}{k_{1l}}\widehat{x} \\ &+(\mu+1)\frac{M_1}{M_2}\frac{k_{2n}}{k_{1l}}\widehat{x}^3 + (\mu+1)\frac{M_1}{M_2}c_2\frac{1}{\sqrt{M_1k_{1l}}}\widehat{x}' = \frac{M_1}{M_2}\mu\frac{f}{k_{1l}}\cos(\Omega\tilde{t}), \end{aligned} \tag{A.5}$$

Because of the conditions of $\frac{M_1}{M_2}\mu = \frac{M_1}{M_2}\frac{M_2}{M_1} = 1$, $\frac{k_{2l}}{k_{1l}} = \frac{M_2}{M_1}\frac{M_1}{M_2}\frac{k_{2l}}{k_{1l}} = \mu\frac{k_{2l}/M_2}{k_{1l}/M_1} = \mu\frac{\omega_2^2}{\omega_1^2} = \mu\gamma^2$ and $\frac{M_1}{M_2}\frac{k_{2n}}{k_{1l}} = \frac{k_{2n}/M_2}{k_{1l}/M_1} = \frac{k_{2n}/M_2}{\omega_1^2} = \frac{k_{2n}}{M_2\omega_1^2}$, Eq. (A.5) is derived as

$$\begin{aligned}
&x_1'' + x_1 + \frac{k_{1n}}{k_{1l}}x_1^3 + c_1\frac{1}{\sqrt{M_1 k_{1l}}}x_1' + \mu\gamma^2\widehat{x} + \frac{k_{2n}}{k_{1l}}\widehat{x}^3 + c_2\frac{1}{\sqrt{M_1 k_{1l}}}\widehat{x}' = \frac{f}{k_{1l}}\cos(\Omega\tilde{t}),\\
&\widehat{x}'' + x_1 + c_1\frac{1}{\sqrt{M_1 k_{1l}}}x_1' + \frac{k_{1n}}{k_{1l}}x_1^3 + (\mu+1)\gamma^2\widehat{x}\\
&+ (\mu+1)\frac{k_{2n}}{M_2\omega_1^2}\widehat{x}^3 + (\mu+1)\frac{M_1}{M_2}c_2\frac{1}{\sqrt{M_1 k_{1l}}}\widehat{x}' = \frac{f}{k_{1l}}\cos(\Omega\tilde{t}),
\end{aligned} \tag{A.6}$$

Introducing the transformation $f \mapsto \frac{f}{k_{1l}}$ and both sides in (A.6) divided by f, (A.6) yields

$$\begin{aligned}
&\frac{x_1''}{f} + \frac{x_1}{f} + \frac{k_{1n}}{k_{1l}}\frac{x_1^3}{f} + c_1\frac{1}{\sqrt{M_1 k_{1l}}}\frac{x_1'}{f} + \mu\gamma^2\frac{\widehat{x}}{f} + \frac{k_{2n}}{k_{1l}}\frac{\widehat{x}^3}{f} + c_2\frac{1}{\sqrt{M_1 k_{1l}}}\frac{\widehat{x}'}{f} = \cos(\Omega\tilde{t}),\\
&\frac{\widehat{x}''}{f} + \frac{x_1}{f} + c_1\frac{1}{\sqrt{M_1 k_{1l}}}\frac{x_1'}{f} + \frac{k_{1n}}{k_{1l}}\frac{x_1^3}{f} + (\mu+1)\frac{M_1}{M_2}\gamma^2\frac{\widehat{x}}{f}\\
&+ (\mu+1)\frac{k_{2n}}{M_2\omega_1^2}\frac{\widehat{x}^3}{f} + (\mu+1)\frac{M_1}{M_2}c_2\frac{1}{\sqrt{M_1 k_{1l}}}\frac{\widehat{x}'}{f} = \cos(\Omega\tilde{t}),
\end{aligned} \tag{A.7}$$

Next, considering the transformation $x_1 \mapsto \frac{x_1}{f}$ and $\widehat{x} \mapsto \frac{\widehat{x}}{f}$, (A.7) is written as

$$\begin{aligned}
&x_1'' + x_1 + \frac{k_{1n}}{k_{1l}}f^2x_1^3 + c_1\frac{1}{\sqrt{M_1 k_{1l}}}x_1' + \mu\gamma^2\widehat{x} + \frac{k_{2n}}{k_{1l}}f^2\widehat{x}^3 + c_2\frac{1}{\sqrt{M_1 k_{1l}}}\widehat{x}' = \cos(\Omega\tilde{t}),\\
&\widehat{x}'' + x_1 + c_1\frac{1}{\sqrt{M_1 k_{1l}}}x_1' + \frac{k_{1n}}{k_{1l}}f^2x_1^3 + (\mu+1)\gamma^2\widehat{x}\\
&+ (\mu+1)\frac{k_{2n}}{M_2\omega_1^2}f^2\widehat{x}^3 + (\mu+1)\frac{M_1}{M_2}c_2\frac{1}{\sqrt{M_1 k_{1l}}}\widehat{x}' = \cos(\Omega\tilde{t}),
\end{aligned} \tag{A.8}$$

Thus, contrasting the coefficients in (A.8) and the dimensionless transformation Eq. (3), Eq. (4) can be obtained.

Appendix B

For the 2DOF vibration system constructed by the primary system and VA with Duffing nonlinearity as Eq. (15), the solutions contain symmetrical terms. For a symmetrical system, only odd harmonics exist in the HBM solution; thus, the solution should be set as

$$\begin{cases}
x_1 = a_1\cos(\Omega\tilde{t}) + \sum_{k=1}^{K}\left[a_{(2k+1)1}\cos((2k+1)\Omega\tilde{t}) + a_{(2k+1)2}\sin((2k+1)\Omega\tilde{t})\right],\\
\widehat{x} = \sum_{k=1}^{K}\left[b_{(2k-1)1}\cos((2k+1)\Omega\tilde{t}) + b_{(2k-1)2}\sin((2k+1)\Omega\tilde{t})\right].
\end{cases} \tag{B.1}$$

The expressions for the nonlinear algebraic equations obtained by HB1 ($K=1$) and HB3 ($K=2$) are given as

$$\begin{aligned}
H_1 = &\left[a_1 - a_1\Omega^2 + \frac{3\alpha_3 a_1^3}{4} + 2\lambda\mu\xi_2\Omega b_{12} + \lambda^2\mu b_{11} + \frac{3\mu\beta_3\lambda^2}{4}\left(b_{11}^3 + b_{11}b_{12}^2\right)\right]^2\\
&+ \left[-\frac{3\mu\beta_3\lambda^2}{4}\left(b_{12}^3 + b_{12}b_{11}^2\right) - \mu\lambda^2 b_{12} + 2\Omega(a_1\xi_1 + \lambda\mu\xi_2 b_{11})\right]^2 = 1,
\end{aligned} \tag{B.2}$$

$$H_{b11} = a_1\Omega^2 + \frac{3}{4}\beta_3\lambda^2\left(b_{11}^3 + b_{11}b_{12}^2\right) - b_{11}\left(\Omega^2 - \lambda^2\right) + 2b_{12}\Omega\lambda\xi_2 = 0, \tag{B.3}$$

$$H_{b12}=\frac{3\beta_3\lambda^2}{4}\left(b_{12}^3+b_{12}b_{11}^2\right)-b_{12}\left(\Omega^2-\lambda^2\right)-2b_{11}\Omega\lambda\xi_2=0, \tag{B.4}$$

and

$$\begin{aligned}H_1=&\left[a_1-a_1\Omega^2+\frac{3\alpha_3}{4}\left(a_1^3+a_1^2a_{31}+2a_1a_{31}^2+a_1a_{32}^2\right)+\lambda^2\mu b_{11}+2b_{12}\Omega\lambda\mu\xi_2\right.\\&\left.+\frac{3\mu\beta_3\lambda^2}{4}\left(b_{11}^3+b_{11}b_{12}^2+b_{11}^2b_{31}-b_{12}^2b_{31}+2b_{11}b_{31}^2+2b_{11}b_{12}b_{32}+2b_{11}b_{32}^2\right)\right]^2\\&+\left[-\frac{3}{4}\alpha_3a_1^2a_{32}+2a_1\Omega\xi_1+2b_{11}\Omega\lambda\mu\xi_2-\mu\lambda^2b_{12}\right.\\&\left.-\frac{3\mu\beta_3\lambda^2}{4}\left(b_{11}^2b_{12}+b_{12}^3+b_{11}^2b_{32}-b_{12}^2b_{32}-2b_{11}b_{12}b_{31}+2b_{12}b_{31}^2+2b_{12}b_{32}^2\right)\right]^2=1,\end{aligned} \tag{B.5}$$

$$\begin{aligned}H_{a31}=&a_{31}-9a_{31}\Omega^2+\frac{\alpha_3a_1^3}{4}+\frac{3\alpha_3}{4}\left(a_{31}a_{32}^2+2a_1^2a_{31}+a_{31}^3\right)+\mu\lambda^2b_{31}+\frac{\beta_3}{4}\mu\lambda^2b_{11}^3\\&+\frac{3\mu\lambda^2\beta_3}{4}\left(-b_{11}b_{12}^2+2b_{11}b_{31}^2+2b_{12}^2b_{31}+b_{31}^3+b_{31}b_{32}^2\right)+6a_{32}\Omega\xi_1+6b_{32}\Omega\lambda\mu\xi_2=0,\end{aligned} \tag{B.6}$$

$$\begin{aligned}H_{a32}=&a_{32}-9a_{32}\Omega^2+\frac{3\alpha_3}{4}\left(a_{32}a_{31}^2+2a_1^2a_{32}+a_{32}^3\right)+\mu\lambda^2b_{32}-\frac{\beta_3}{4}\mu\lambda^2b_{12}^3\\&+\frac{3\mu\lambda^2\beta_3}{4}\left(b_{12}b_{11}^2+2b_{32}b_{32}^2+2b_{11}^2b_{32}+b_{32}^3+b_{32}b_{31}^2\right)+6a_{31}\Omega\xi_1+6b_{31}\Omega\lambda\mu\xi_2=0,\end{aligned} \tag{B.7}$$

$$\begin{aligned}H_{b11}=&a_1\Omega^2-b_{11}\Omega^2+b_{11}\lambda^2+2b_{12}\Omega\lambda\mu\xi_2\\&+\frac{3\beta_3\lambda^2}{4}\left(b_{11}^3+b_{11}b_{12}^2+b_{11}b_{31}^2-b_{12}^2b_{31}+2b_{11}b_{31}^2+2b_{11}b_{12}b_{32}+2b_{11}^2b_{32}\right),\end{aligned} \tag{B.8}$$

$$\begin{aligned}H_{b12}=&-b_{12}\Omega^2+b_{12}\lambda^2-2b_{11}\Omega\lambda\mu\xi_2\\&+\frac{3\beta_3\lambda^2}{4}\left(b_{12}^3+b_{12}b_{11}^2+b_{11}b_{32}^2-b_{12}^2b_{32}+2b_{12}b_{32}^2-2b_{11}b_{12}b_{31}+2b_{11}^2b_{32}\right),\end{aligned} \tag{B.9}$$

$$\begin{aligned}H_{b31}=&a_{31}-9a_{31}\Omega^2+\frac{\alpha_3a_1^2}{4}+\frac{3\alpha_3}{4}\left(a_{31}a_{32}^2+2a_1^2a_{31}+a_{31}^3\right)+(\mu+1)\lambda^2b_{31}+\frac{\beta_3}{4}(\mu+1)\lambda^2b_{11}^3\\&+\frac{3(\mu+1)\lambda^2\beta_3}{4}\left(-b_{11}b_{12}^2+2b_{11}b_{31}^2+2b_{12}^2b_{31}+b_{31}^3+b_{31}b_{32}^2\right)+6(\mu+1)b_{32}\Omega\xi_1=0,\end{aligned} \tag{B.10}$$

$$\begin{aligned}H_{b32}=&a_{32}-9a_{32}\Omega^2+\frac{3\alpha_3}{4}\left(a_{32}a_{31}^2+2a_1^2a_{32}+a_{32}^3\right)+(\mu+1)\lambda^2b_{32}-\frac{\beta_3}{4}(\mu+1)\lambda^2b_{12}^3\\&+\frac{3(\mu+1)\lambda^2\beta_3}{4}\left(b_{12}b_{11}^2+2b_{32}b_{32}^2+2b_{11}^2b_{32}+b_{32}^3+b_{32}b_{31}^2\right)+6(\mu+1)b_{31}\Omega\xi_1=0,\end{aligned} \tag{B.11}$$

respectively.

Appendix C

For the fitting polynomial g_1 with multiple terms, the coefficients are obtained by the LSM. For different values of motion $\widehat{x}_k$ ($k=1,2,\ldots,N$), the original restoring force obeys Eq. (19), equalling to $G_1(\widehat{x}_k)$. Utilizing fitting polynomial g_1 to fit these points $(\widehat{x}_k, G_1(\widehat{x}_k))$, the error between g_1 and these points should be minimum, which is given by the following condition.

$$I = \sum_{k}^{N} [g_1(\hat{x}_k) - G_1(\hat{x}_k)]^2$$
$$= \sum_{k}^{N} \left[k_{1l}\hat{x}_k + \sum_{j=1}^{J} k_{1n(2j+1)}\hat{x}_k^{2j+1} - k_v\hat{x}_k - 2k_h\hat{x}_k \left(1 - \frac{l_0}{\sqrt{(l_0-\lambda_0)^2 + \hat{x}_k^2}} \right) \right]^2 = \min. \tag{C.1}$$

Thus, the fitting processing is the solution of an extremum problem. The coefficients $k_{1n(2j+1)}$ $(j = 0,1,2,\ldots,J)$ are obtained by

$$\frac{\partial I}{\partial k_{1n(2j+1)}} = 0. \quad j = 0, 1, 2, \ldots, J. \tag{C.2}$$

Then, we have $J+1$ equations for the $J+1$ coefficients $k_{1l} = \mathrm{k}_{1n1}$ and $\mathrm{k}_{1n(2j+1)}$.
On the other hand, the coefficients of Taylor series expansion are expressed as

$$\sum_{j=0}^{J} \frac{G_1^{(2j+1)}}{j!} \hat{x}^{(2j+1)} \tag{C.3}$$

Fig. C.1 shows the comparison of the polynomial function g_1 and the Taylor series expansion with same order $i = 15$. In the comparison in Fig. 11, without loss of generality, the structural parameters are $k_v = 1$, $k_h = 0.5$, and $l_0 = 1$.

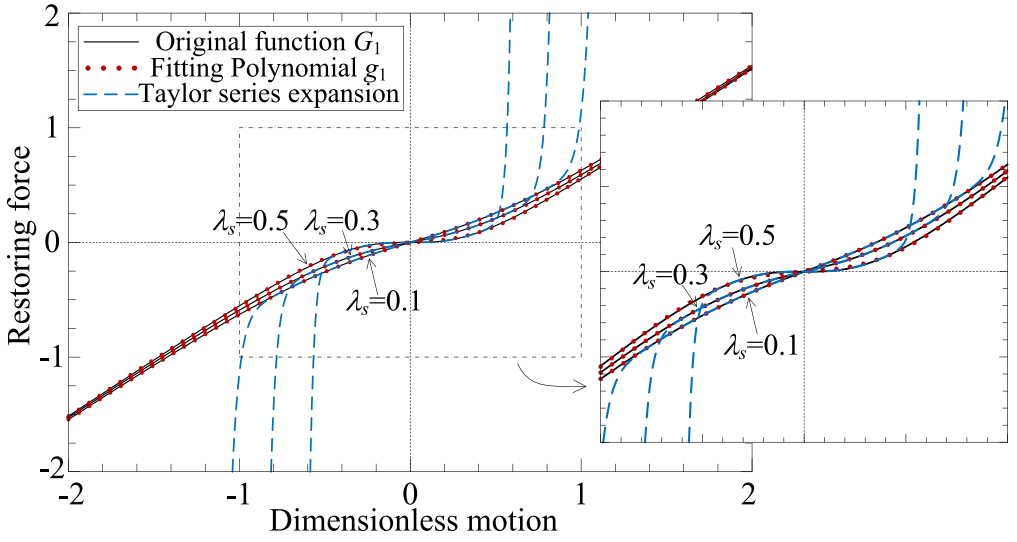

Fig. C.1. Comparison of the restoring force functions among the original function G_1, fitting polynomial g_1 and Taylor series expansion.

Appendix D

The experiment of the primary system with QZS property is shown in Fig. D. 1.

Table 1
The fitting polynomial g_1 for different λ_s.

λ_s	g_1
0.0	$1.004\hat{x}_1 + 0.46\hat{x}_1^3 - 0.253\hat{x}_1^5 + 0.11\hat{x}_1^7 - 0.035\hat{x}_1^9 + 0.008\hat{x}_1^{11} - 0.0014\hat{x}_1^{13} + 1.71\times10^{-4}\hat{x}_1^{15}$ $-1.6\times10^{-5}\hat{x}_1^{17} + 1.11\times10^{-6}\hat{x}_1^{19} - 5.68\times10^{-8}\hat{x}_1^{21} + 2.04\times10^{-9}\hat{x}_1^{23} - 4.43\times10^{-11}\hat{x}_1^{25} + 1.15\times10^{-13}\hat{x}_1^{27}$ $+3.02\times10^{-14}\hat{x}_1^{29} - 1.2\times10^{-15}\hat{x}_1^{31} + 2.5\times10^{-17}\hat{x}_1^{33} - 3.2\times10^{-19}\hat{x}_1^{35} + 2.34\times10^{-21}\hat{x}_1^{37} - 7.6\times10^{-24}\hat{x}_1^{39}$
0.1	$0.898\hat{x}_1 + 0.6\hat{x}_1^3 - 0.37\hat{x}_1^5 + 0.17\hat{x}_1^7 - 0.057\hat{x}_1^9 + 0.013\hat{x}_1^{11} - 0.002\hat{x}_1^{13} + 2.8\times10^{-4}\hat{x}_1^{15}$ $-2.7\times10^{-5}\hat{x}_1^{17} + 1.89\times10^{-6}\hat{x}_1^{19} - 9.75\times10^{-8}\hat{x}_1^{21} + 3.52\times10^{-9}\hat{x}_1^{23} - 7.67\times10^{-11}\hat{x}_1^{25} + 2.09\times10^{-13}\hat{x}_1^{27}$ $+5.22\times10^{-14}\hat{x}_1^{29} - 2.07\times10^{-15}\hat{x}_1^{31} + 4.37\times10^{-17}\hat{x}_1^{33} - 5.6\times10^{-19}\hat{x}_1^{35} + 4.09\times10^{-21}\hat{x}_1^{37} - 1.3\times10^{-24}\hat{x}_1^{39}$
0.2	$0.767\hat{x}_1 + 0.8\hat{x}_1^3 - 0.55\hat{x}_1^5 + 0.27\hat{x}_1^7 - 0.091\hat{x}_1^9 + 0.022\hat{x}_1^{11} - 0.0038\hat{x}_1^{13} + 4.8\times10^{-4}\hat{x}_1^{15}$ $-4.6\times10^{-5}\hat{x}_1^{17} + 3.24\times10^{-6}\hat{x}_1^{19} - 1.67\times10^{-8}\hat{x}_1^{21} + 6.05\times10^{-9}\hat{x}_1^{23} - 1.33\times10^{-11}\hat{x}_1^{25} + 3.77\times10^{-13}\hat{x}_1^{27}$ $+8.98\times10^{-14}\hat{x}_1^{29} - 3.59\times10^{-15}\hat{x}_1^{31} + 7.56\times10^{-17}\hat{x}_1^{33} - 9.67\times10^{-19}\hat{x}_1^{35} + 7.1\times10^{-21}\hat{x}_1^{37} - 2.3\times10^{-24}\hat{x}_1^{39}$
0.3	$0.607\hat{x}_1 + 1.1\hat{x}_1^3 - 0.81\hat{x}_1^5 + 0.42\hat{x}_1^7 - 0.15\hat{x}_1^9 + 0.036\hat{x}_1^{11} - 0.0063\hat{x}_1^{13} + 8.16\times10^{-4}\hat{x}_1^{15}$ $-7.8\times10^{-5}\hat{x}_1^{17} + 5.5\times10^{-6}\hat{x}_1^{19} - 2.85\times10^{-8}\hat{x}_1^{21} + 1.04\times10^{-9}\hat{x}_1^{23} - 2.28\times10^{-11}\hat{x}_1^{25} + 6.74\times10^{-13}\hat{x}_1^{27}$ $+1.54\times10^{-14}\hat{x}_1^{29} - 6.17\times10^{-15}\hat{x}_1^{31} + 1.3\times10^{-17}\hat{x}_1^{33} - 1.67\times10^{-19}\hat{x}_1^{35} + 1.23\times10^{-21}\hat{x}_1^{37} - 4.01\times10^{-24}\hat{x}_1^{39}$
0.4	$0.406\hat{x}_1 + 1.48\hat{x}_1^3 - 1.21\hat{x}_1^5 + 0.66\hat{x}_1^7 - 0.24\hat{x}_1^9 + 0.059\hat{x}_1^{11} - 0.0105\hat{x}_1^{13} + 1.36\times10^{-3}\hat{x}_1^{15}$ $-1.31\times10^{-4}\hat{x}_1^{17} + 9.3\times10^{-6}\hat{x}_1^{19} - 4.84\times10^{-7}\hat{x}_1^{21} + 1.76\times10^{-8}\hat{x}_1^{23} - 3.\times10^{-10}\hat{x}_1^{25} + 1.19\times10^{-12}\hat{x}_1^{27}$ $+2.62\times10^{-13}\hat{x}_1^{29} - 1.06\times10^{-14}\hat{x}_1^{31} + 2.23\times10^{-17}\hat{x}_1^{33} - 2.87\times10^{-18}\hat{x}_1^{35} + 2.11\times10^{-20}\hat{x}_1^{37} - 6.89\times10^{-23}\hat{x}_1^{39}$
0.5	$0.152\hat{x}_1 + 2.05\hat{x}_1^3 - 1.82\hat{x}_1^5 + 1.03\hat{x}_1^7 - 0.38\hat{x}_1^9 + 0.096\hat{x}_1^{11} - 0.017\hat{x}_1^{13} + 2.26\times10^{-3}\hat{x}_1^{15}$ $-2.18\times10^{-4}\hat{x}_1^{17} + 1.56\times10^{-5}\hat{x}_1^{19} - 8.14\times10^{-7}\hat{x}_1^{21} + 2.98\times10^{-8}\hat{x}_1^{23} - 6.61\times10^{-10}\hat{x}_1^{25} + 2.09\times10^{-12}\hat{x}_1^{27}$ $+4.43\times10^{-13}\hat{x}_1^{29} - 1.79\times10^{-14}\hat{x}_1^{31} + 3.8\times10^{-16}\hat{x}_1^{33} - 4.88\times10^{-18}\hat{x}_1^{35} + 3.59\times10^{-20}\hat{x}_1^{37} - 1.18\times10^{-22}\hat{x}_1^{39}$

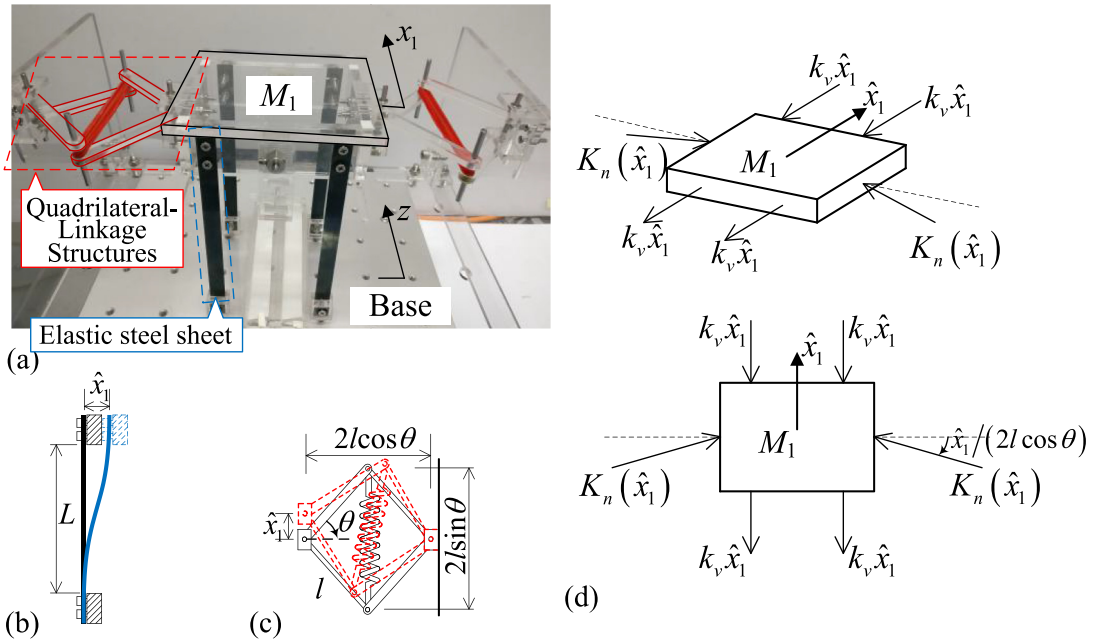

Fig. D.1. (a) Experimental prototype of the primary system with QZS property, (b) deformations of elastic steel sheet, (c) deformation of the right-side QLS, and (d) force diagram of the isolation object.

Fig. D. 1 (a) shows the nonlinear primary system for the experiments. According to Ref. [34], in Fig. D. 1 (a), the elastic steel sheets act as a positive stiffness component, and the pre-deformation symmetrical assembled Quadrilateral-Linkage Structures acts as the negative stiffness component. For motion $\hat{x}_1$, the elastic steel sheets are curved laterally, as shown in Fig. D. 1 (b), and the Quadrilateral-Linkage Structure deforms as shown in Fig. D. 1 (c). Then, the restoring force of the primary system is nonlinear, which is shown in Fig. D. 1 (d). The experimental prototype of the proposed isolation primary system can realize the High-Static-Low-Dynamic property because of the adjustable nonlinear stiffness. This kind of vibration system is widely applied in vibration isolation fields due to the high-static-low-frequency property induced by the complex nonlinear restoring force. Based on Refs. [29–34], the dynamical equation of the proposed nonlinear primary system shown in Fig. D. 1 (a) is written as

$$M_1\ddot{\hat{x}}_1 + k_{1l}\hat{x}_1 + \sum_{j=1}^{n} k_{1n(2j+1)}\hat{x}_1^{2j+1} + c_1\dot{\hat{x}}_1 = 0. \tag{D.1}$$

Appendix E. Supplementary data

Supplementary data to this article can be found online at https://doi.org/10.1016/j.jsv.2019.02.033.

References

[1] R.A. Ibrahim, Recent advances in nonlinear passive vibration isolators, J. Sound Vib. 314 (2008) 371–452.
[2] A. Carrella, M.J. Brennan, T.P. Waters, V. Lopes Jr., Force and displacement transmissibility of a nonlinear isolator with high-static-low-dynamic-stiffness, Int. J. Mech. Sci. 55 (1) (2012) 22–29.
[3] S.Y. Xia, D.L. Xu, H.C. Zhang, et al., On retaining a multi-module floating structure in an amplitude death state, Ocean Eng. 121 (2016) 134–142.
[4] H.C. Zhang, D.L. Xu, C. Lu, E.R. Qi, J.J. Hu, Y.S. Wu, Amplitude death of a multi-module floating airport, Nonlinear Dynam. 79 (4) (2015) 2385–2394.
[5] Q. Ran, M.L. Xiao, Y.X. Hu, Nonlinear vibration with volterra series method used in civil engineering: the Bouc-Wen hysteresis model of generalized frequency response, Appl. Mech. Mater. 530–531 (2014) 561–566.
[6] A.F. Vakakis, O.V. Gendelman, L.A. Bergman, Nonlinear Targeted Energy Transfer in Mechanical and Structural Systems, Springer Netherlands, 2009.
[7] H. Jo, H. Yabuno, Amplitude reduction of primary resonance of nonlinear oscillator by a dynamic vibration absorber using nonlinear coupling, Nonlinear Dynam. 55 (1–2) (2009) 67–78.
[8] R. Viguie, G. Kerschen, Nonlinear vibration absorber coupled to a nonlinear primary system: a tuning methodology, J. Sound Vib. 326 (3–5) (2009) 780–793.
[9] G. Habib, C. Grappasonni, G. Kerschen, Passive linearization of nonlinear resonances, J. Appl. Phys. 120 (4) (2016) 044901.
[10] P.G. Dylejko, I.R. Macgillivray, On the concept of a transmission absorber to suppress internal resonance, J. Sound Vib. 333 (10) (2014) 2719–2734.
[11] Y. Du, R.A. Burdisso, E. Nikolaidis, Control of internal resonances in vibration isolators using passive and hybrid dynamic vibration absorbers, J. Sound Vib. 286 (2005) 697–727.
[12] A. Vyas, A.K. Bajaj, Dynamics of autoparametric vibration absorbers using multiple pendulums, J. Sound Vib. 246 (1) (2001) 115–135.
[13] R.J. Monroe, S.W. Shaw, Nonlinear transient dynamics of pendulum torsional vibration absorbers, J. Vib. Acoust. 135 (1) (2013) 011018.
[14] P.G. Dylejko, I.R. Macgillivray, On the concept of a transmission absorber to suppress internal resonance, J. Sound Vib. 333 (10) (2014) 2719–2734.
[15] J.C. Ji, Design of a nonlinear vibration absorber using three-to-one internal resonances, Mech. Syst. Signal Process. 42 (1–2) (2014) 236–246.
[16] M. Sayed, M. Kamel, 1:2 and 1:3 internal resonance active absorber for non-linear vibrating system, Appl. Math. Model. 36 (1) (2012) 310–332.
[17] D. Zulli, A. Luongo, Nonlinear energy sink to control vibrations of an internally nonresonant elastic string, Meccanica 50 (3) (2015) 781–794.
[18] R. Viguié, G. Kerschen, J.C. Golinval, Using passive nonlinear targeted energy transfer to stabilize drill-string systems, Mech. Syst. Signal Process. 23 (1) (2009) 148–169.
[19] M.A. Al-Shudeifat, N.E. Wierschem, L.A. Bergman, Numerical and experimental investigations of a rotating nonlinear energy sink, Meccanica 52 (4–5) (2017) 763–779.
[20] Q.J. Cao, T.D. Zhang, J.P. Li, A study of the static and global bifurcations for Duffing equation, Appl. Math. Mech. 20 (12) (1999) 1413–1420.
[21] Y.L. Cheung, W.O. Wong, L. Cheng, Design optimization of a damped hybrid vibration absorber, J. Sound Vib. 331 (4) (2012) 750–766.
[22] T. Asami, O. Nishihara, Closed-form exact solution to H∞ optimization of dynamic vibration absorbers (application to different transfer functions and damping systems), J. Vib. Acoust. 125 (3) (2003) 398–405.
[23] J.P. Den Hartog, Mechanical Vibration, McGraw-Hill, New York, 1934.
[24] G. Habib, T. Detroux, R. Viguié, Nonlinear generalization of Den Hartog's equal-peak method, Mech. Syst. Signal Process. 52–53 (1) (2015) 17–28.
[25] T. Detroux, G. Habib, L. Masset, G. Kerschen, Performance, robustness and sensitivity analysis of the nonlinear tuned vibration absorber, Mech. Syst. Signal Process. 60–61 (2015) 799–809.
[26] L. Dell'Elce, E. Gourc, G. Kerschen, A robust equal-peak method for uncertain mechanical systems, J. Sound Vib. 414 (2018) 97–109.
[27] Y.L. Cheung, W.O. Wong, L. Cheng, Design optimization of a damped hybrid vibration absorber, J. Sound Vib. 331 (4) (2012) 750–766.
[28] A.H. Nayfeh, D.T. Mook, Nonlinear Oscillations, Wiley-Interscience, New York, 1979.
[29] I. Kovacic, M.J. Brennan, T.P. Waters, A study of a nonlinear vibration isolator with a quasi-zero-stiffness characteristic, J. Sound Vib. 315 (3) (2008).
[30] J. Zhou, X. Wang, D. Xu, S. Bishop, Nonlinear dynamic characteristics of a quasi-zero stiffness vibration isolator with cam–roller–spring mechanisms, J. Sound Vib. 346 (1) (2015) 53–69.
[31] G. Gatti, I. Kovacic, M.J. Brennan, On the response of a harmonically excited two degree-of-freedom system consisting of a linear and a nonlinear quasi-zero stiffness oscillator, J. Sound Vib. 329 (10) (2010) 1823–1835.
[32] X. Wang, H. Liu, Y. Chen, P. Gao, Beneficial stiffness design of a high-static-low-dynamic-stiffness vibration isolator based on static and dynamic analysis, Int. J. Mech. Sci. 142–143 (2018) 235–244.
[33] Y. Zheng, X. Zhang, Y. Luo, Y. Zhang, S. Xie, Analytical study of a quasi-zero stiffness coupling using a torsion magnetic spring with negative stiffness, Mech. Syst. Signal Process. 100 (2018) 135–151.
[34] F. Wang, X. Sun, J. Xu, A novel energy harvesting device for ultralow frequency excitation, Energy 151 (2018) 250–260.
[35] S. Waitukaitis, R. Menaut, B.G. Chen, Origami multistability: from single vertices to metasheets, Phys. Rev. Lett. 114 (2014) 055503.
[36] X. Sun, S. Zhang, J. Xu, A Novel isolation structure with flexible joints for impact and ultralow-frequency excitations, Int. J. Mech. Sci. 146 (2018) 366–376.